Automation of Stem Cell Protocols

A THESIS SUBMITTED TO THE FACULTY OF THE UNIVERSITY OF MINNESOTA BY:

BLAKE LEON JOHNSON

IN PARTIAL FULFILLMENT OF THE REQUIREMENTS FOR THE DEGREE OF MASTER OF SCIENCE

FACULTY ADVISOR:
JAMES DUTTON, PhD

University of Minnesota - Twin Cities

December 2019

Acknowledgements

I have many people that I must thank for help in completing this research. They are as follows:

James R. Dutton, PhD, for guiding me in these experiments, for working cooperatively to accomplish my goals, and for inspiring passion into this research.

Susan A. Keirstead, PhD, for keeping me on schedule, pushing me to further my data interpretation skills, and for being an amazing program advisor.

Rui Li, for being an incredible partner in this research, for always working with me to overcome complications and errors that arise, and for always being available for help and guidance.

Vincent Truong, for teaching me how to work the automated platform, as well as working cooperatively to critically solve many problems and issues that have arose. This research would not have been possible without your detailed knowledge of this technology.

Patrick Walsh, for informing me on the finer details to neuronal differentiation and maintenance.

Aimee Renaud, Noah Denman, Olivia Hood, Isaias Roberson, and Kevin Viken, for support and amazing teamwork so we all could accomplish our goals.

Abstract

Human induced pluripotent stem cells (hiPSCs) have become a vital resource for researchers and industry due to their differentiation capacity, as well as providing access to the cell phenotypes and genotypes from any individual donor. Despite improvements in stem cell technology, maintaining iPS cell lines still requires a significant amount of time and technical skill from cell culture technicians. Such steps include consistent media changes, cell counting and confluence analyses, cell passaging, cryopreservation, and subsequent thawing and plating of those cells. For this research, these processes have been transitioned onto an automated cell culturing platform. It is shown here that the automated cell culturing platform is able to properly execute DMSO-free cryopreservation, thawing, plating, and cell maintenance. This demonstrated ability to perform these functions completely automated without a technician is a technical advancement in pluripotent stem cell culturing and may provide financial benefits within a cell culture laboratory.

Table of Contents

Table of Figures, Tables, and Equations

Introduction

Background

Utilizing the technology of reprogramming human adult somatic cells induced pluripotent stem cells (hiPSCs) has become a vital resource for researchers and industry professionals due to their differentiation capacity, as well as providing access to the phenotypes and genotypes from any individual donor[1]. Despite improvements in stem cell technology including the introduction of defined media and growth substrates that have replaced the use of undefined reagents and feeder cell layers in the culture of human pluripotent stem cells, maintaining iPS cell lines still requires a significant amount of time and technical skill from cell culture technicians. Such steps include consistent media changes, cell counting and confluence analyses, cell passaging, cryopreservation and subsequent thawing and plating of those cells. Manual interference in cell culturing also increases chances of contamination. Implementation of automated systems is a potential solution to address these issues.

Automation is becoming a more commonly used tool within cell biology. The implementation of these systems is due to the benefits of an enclosed system compared to a technician manually maintaining the cell cultures[2]; such benefits include an improved sterility setting, consistent procedure execution, and less variability. Scaling up production may also be quicker utilizing these platforms, thereby reducing the time to market. Further, the ability to maintain cells in culture without manual intervention may reduce the effort of cell culture technicians. Even with these benefits, implementation of these systems has not been fully integrated in the cell culturing industry, primarily due to a high upfront cost. Research that validates and demonstrates the abilities of these platforms are a necessity for adaptation within the industry.

Automated Platforms For Cell Culture

In recent years there has been major development of many new platforms for automated cell culture and demonstration of the abilities of these systems has continually been improving. In 2007 it was demonstrated an automated media-changing system for flask human mesenchymal stem cell cultures using a four-axis robot[3]. Several companies,

such as Sartorius, Beckman Coulter, Tecan[4], and Hamilton Robotics[5] have designed a version of an automated cell culturing platform that has the ability to perform adherent cell culture. Representative images of available platforms can be seen in Figure 1. Figure 1A shows Sartorius' ambr® 15 cell culture system, which can perform automated liquid handling with standard plate formats along with the added benefit of incorporating microbioreactor culture. The liquid handling uses air displacement for pipette control, which is widely used and standard as an accurate method for pipetting. With this,

Figure 1:

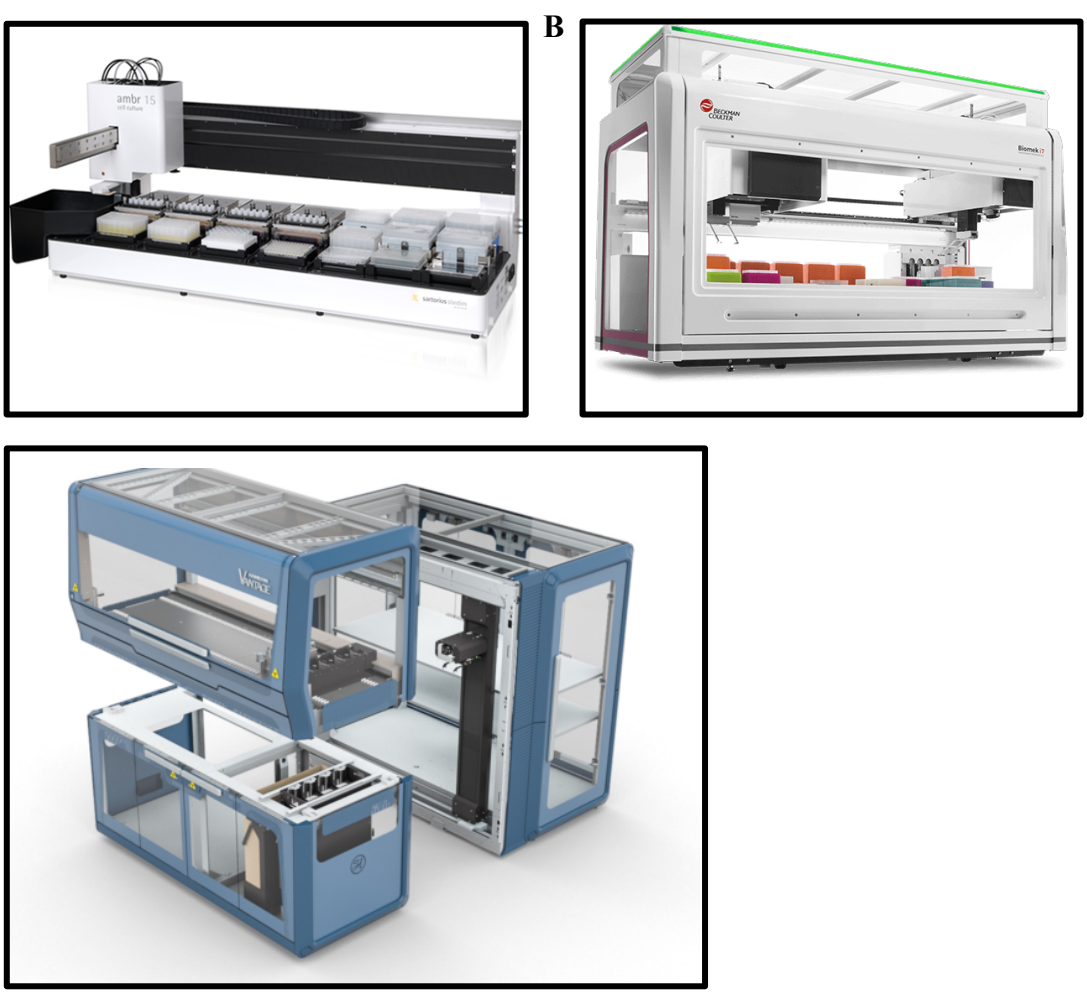

Figure 1: Representative images of currently available automated cell culture workstations (A): Sartorius' ambr® 15 cell culture system (B): Beckman Coulter's Biomek i7 automated workstation (C): Hamilton's VANTAGE automated workstation. Photos retrieved from:
(A): https://www.sartorius-stedim-tap.com/tap/cell_culture/ambr.htm
(B): https://www.beckman.com/liquid-handlers/biomek-i7
(C): https://www.hamiltoncompany.com/automated-liquid-handling/platforms/microlab-vantage-liquid-handling-system

automated liquid transfers are possible to perform many functions such as media exchange or drug delivery. The Biomek i7 automated workstation created by Beckman Coulter is shown in Figure 1B. This workstation, along with Hamilton's VANTAGE workstation as shown in Figure 1C, can perform automated liquid handling and can incorporate third party modules. Integrating third party modules is an important feature to expand the capabilities of automation. These can include incubators, imaging microscopes, heating and cooling blocks, as well as other more specialized modules.

TECAN Fluent Platform

The automation platform that is used in these experiments was the Tecan Fluent laboratory automation workstation. There have already been applications of the Tecan Fluent laboratory automation workstation within drug discovery, high throughput screens, and subsequently drug testing, research[7]. One example that demonstrated the use of the Tecan Fluent was in discovering antiviral leads that were derived from complex traditional Chinese medicine[8]. The Tecan Fluent automation platform is a new generation workstation that has evolved from the TECAN EVO Freedom workstation. A photo of the Tecan Fluent automation platform is shown in Figure 2A, while a design and equipment layout of the Fluent workstations used for this project are described in Figure 2B.

The Fluent is well-equipped to perform the necessary functions for maintaining cells in adherent culture. The worktable is encased in a Biosafety cabinet, complete with HEPA filtering to allow for a clean cell culturing space. Within the space and above the worktable are three mobile arms that can navigate throughout the space. These include the Air LiHa (Liquid Handling) arm, otherwise referred to as the Fluid Channel Arm (FCA), which can retrieve pipetting tips to allow for aspiration and dispensing of liquids. The option to replace the Air LiHa, an air-displacement pipetting method, for the Liquid LiHa, a positive-displacement pipetting method, is available. For situations that utilize a 96-well or 384-well plate, there is a MultiChannel Arm (MCA) that attaches pipette tips for liquid volume manipulation within that plate format. Lastly, there is a Robot Gripper Arm (RGA) that has multiple 'fingers' that give it the capability to move and grip labware from plates, to lids, to even tubes. This arm allows for plates to be moved around the workstation including from the incubator, to the workstation deck and to the tilt carrier, or to the BioTek

Figure 2:

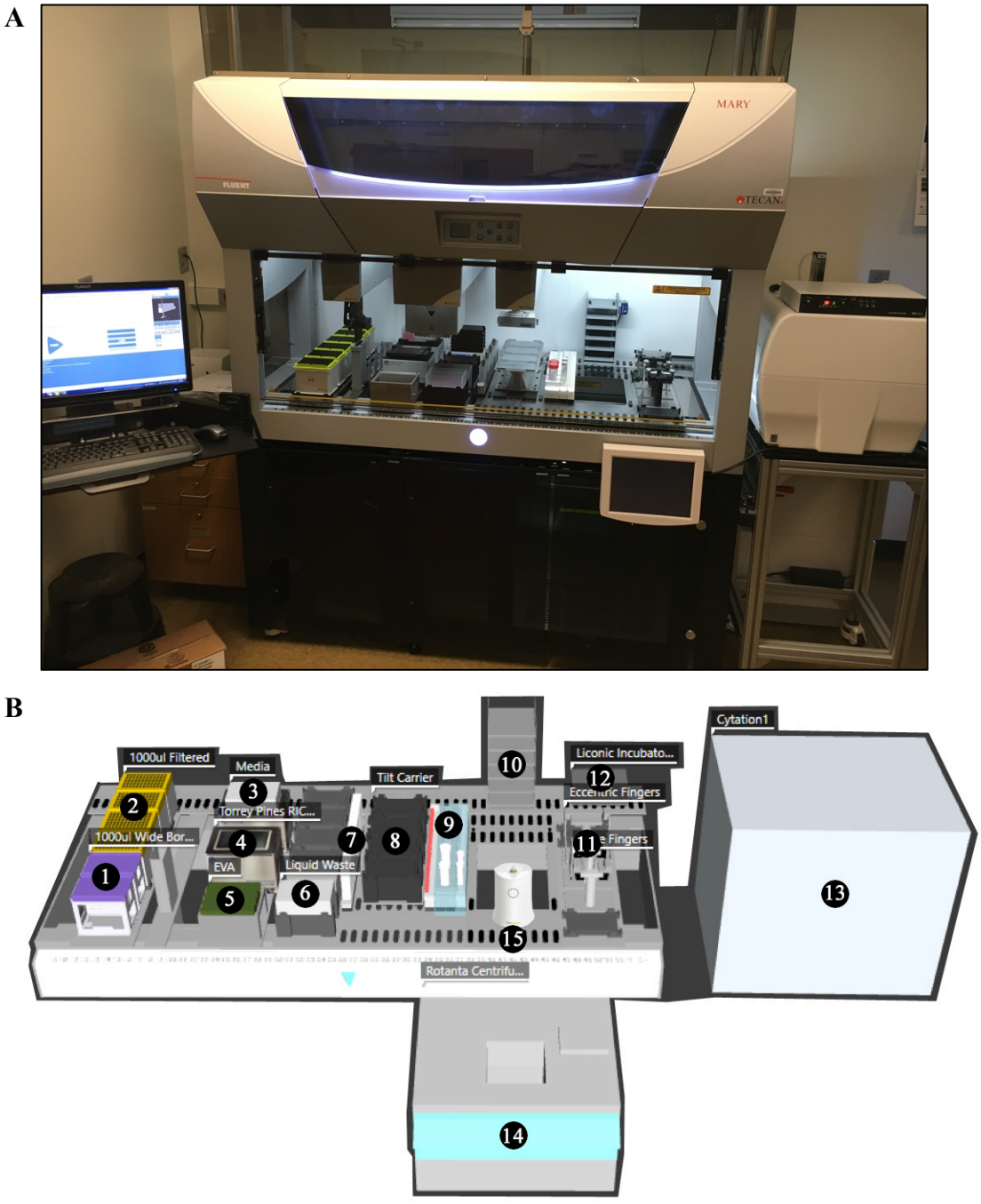

Figure 2: An overview of the Tecan Fluent 780 automated workstation used for this project (A): A photo of the Tecan Fluent 780 automated workstation. (B): A Tecan Fluent-generated image of the work deck and numbered sections: (1) Wide bore 1000uL tips (2) 1000uL tips (3-4) Media trough & Torrey Pines heating / cooling element (5) MCA head 96-well adapter (6) Media waste (7) Liquid rack (8) Tilt Carrier (9) Tube rack (10) Hotel (11) 3 RGA finger adapters (12) Transport to incubator (13) BioTek CytoOne imaging station (14) Centrifuge (15) Biocision ThawStar.

Cytation, where automated imaging can be performed. A segmented runner deck allows for easy incorporation of third party modules and once properly connected they are able to communicate between each other and the Fluent software. The tilt carrier is one example of this kind of module. The number of tilts, angle, and speed of the tilts can all be programmed within a script. Media can be stored on the worktable in lidded troughs which are temperature controlled via the Torrey Pines heating and cooling stations; the temperature of these stations can be incorporated into the control script if protocols call for heating of the media or if the media/ supplements need to be kept below room temperature. There is also an integrated automated centrifuge below the worktable. Other modules can be incorporated into the worktable, which could further expand the capabilities of this system. However, additional programming and trouble-shooting is required to confidently incorporate additional equipment into reliable scripts.

Tecan Fluent Control is the proprietary software package used to control the Fluent platform; the FluentControl software is a graphical user interface, intuitive for users to design and program scripts that can then be executed. Procedures pertinent to cell culture can be programmed and linked as functioning scripts including brightfield imaging, media change, cell passaging, and addition of defined volumes of media components required for cell differentiations. These tasks are performed using the robotic gripper arms and pipetting heads and a worktable equipped with various peripheral equipment options.

Adding Additional Capabilities

Exploring more protocols that can be implemented onto this automated platform is necessary in proving additional potential capabilities. This project has focused on developing additional protocols for automating cryopreservation, as well as post-preservation cell thawing and plating, critical for assessing post-thaw viability. Implementing these methods will allow progress on developing end-to-end automation protocols for plating cells, maintaining and expanding them, and implementing cryopreservation with minimal human interaction. Cell differentiation can be implemented within this process so that cryopreservation is of the resulting differentiated cell type. These procedures will expand the current scripted capabilities of our workstations.

Cryopreservation

Cryopreservation is a necessary protocol for preparing cells for conservation at low temperatures. The stock of preserved cells serves as the method for long term cell storage, as reserve cells to replace cells in culture and as a method for transporting cells[9]. The cryopreservation process utilizes liquid nitrogen for low temperatures, usually below -196°C to preserve and store living cells, while maintaining its structural integrity. Under normal, uncontrolled freezing conditions, the development of ice crystals can mechanically destroy the cells, specifically the development of intracellular ice is significantly lethal[10,11]. There are other theories as to why freezing can be damaging, which include an irregular tonicity[12], as well as membrane stress[13,14] resulting from the reduction in volume occurring during freezing. These negative effects can be prevented by integrating a cryoprotectant reagent with the cells before freezing. These cryoprotectants achieve the goals of cryopreservation by preventing intracellular freezing and attaining intracellular vitrification. The first cryopreservation method used was in 1949, when researchers revived human spermatozoa cells utilizing glycerol as the cryoprotectant[15]. Ten years later in 1959 Lovelock demonstrated the use of DMSO as a cryoprotectant to address the issue that certain cell types are impermeable to glycerol[14-16]. Since the first demonstration in 1959, DMSO had eventually been adopted as a standard cryoprotectant reagent.

Effects of DMSO

Even though it is an effective and standard cryoprotectant, DMSO has been shown to have a toxic effect towards cells. There have been a number of reports demonstrating the negative effects of DMSO on multiple cell types[17-19]. Apoptosis has been highlighted as one major effect of exposure on several cell types. Galvao demonstrated in their research that rat retinal cells exposed to concentrations of DMSO below 10% were subject to apoptosis[17]. Their results also showed a direct correlation with the amount of DMSO used and the amount of apoptosis induced. Hanslick also demonstrated similar correlated apoptotic results when exposing developing mouse central nervous tissue to DMSO[18].

Beyond apoptosis-induced cell death, DMSO had also been shown to diminish production of OCT-4 in human embryonic stem cells[19]. After three days of culture after being frozen with DMSO as a cryoprotectant reagent there was 50% viability and only 10% of EGFP-positive expression where EGFP reporter expression was driven by an OCT-4

promoter. Recently, there has been evidence that DMSO leads to modifications in miRNA and other genome-wide epigenetic changes such as methylation in cardiomyocytes generated from induced pluripotent stem cells[20]. Retaining all of the characteristics of the original cells is the ultimate goal for cryopreservation, and DMSO is not completely fulfilling this goal.

Alternative Cryopreservation Reagents

Alternative methods incorporating different cryopreservation reagents are being developed. An alternative cryopreservation reagent to DMSO may be important for utilizing human cells in a clinical setting. There have been many studies demonstrating the possibility of incorporating other cryoprotectant reagents as a replacement to DMSO. Some examples include carbohydrate cryoprotectant agents such as glycerol, propylene glycol, ethylene glycol, sucrose, and trehalose[21]. The problem with these agents compared to DMSO is that they are unable to penetrate the cell membrane, therefore intracellular vitrification is unable to occur. An example of a demonstrated DMSO-alternative is the use of polyampholytes, which are macromolecules containing carboxyl (acidic) and amino (basic) groups that dissociate in aqueous solutions[22]. Using this as a cryopreservation reagent resulted in similar cell viability as DMSO-based cryopreservation[23]. Svalgaard demonstrated the use of pentaisomaltose to cryopreserve hematopoietic progenitor cells[24]. The researchers presented data that showed similar percentages of recovery of viable cells compared to DMSO in cord blood cell types, which include granulocytes and CD34+ cells. Pollock used an innovative method of finding the optimal cryopreservation solution composition by utilizing a differential evolution algorithm[25]. They found a combination of trehalose, glycerol, and ectoine to preserve Jurkat lymphoblastoid cells, while for mesenchymal stem cells a combination of ethylene glycol, taurine, and ectoine was preferable. The same researchers used an algorithm to find the optimal cryopreservation solution for a human induced pluripotent stem cell line. This proprietary composition is used in the research presented here to demonstrate an automated DMSO-free cryopreservation method.

Automating this cryopreservation procedure would be useful for incorporating this process in cell culture maintenance. This demonstratable ability to be completely

performed without the use of a technician is also a benefit that is outside of the scientific benefits and could impact the financial benefits that a laboratory may use. Further, this technique could be incorporated into a much larger protocols such as end to end patient-specific iPSC-based drug screening.

Automating hiPSC-Differentiation Protocols and PARs

The focus of this part of the project has been in support of research being performed in relation to assessing the effect of inhibiting protease activated receptor activity on neural stem cell and neural precursor growth and differentiation. Protease-activated receptors (PARs) were initially found in platelets, fibroblasts, and endothelial cells[26], but have also been found to have an important role within the peripheral nervous system and the central nervous system[28]. There are four different types of PARs, which are known as PAR-1 - 4. All four of the different PARs are expressed in neurons in both the central and peripheral nervous systems, and control neurotransmitter release, ion channel activity, cell survival, and cell morphology [28]. These receptors have significant roles in inflammation pathways, as well as neural degenerative diseases like dementia and Alzheimer's. There is also a potential that the PARs could have importance in the pathogenesis of Parkinson's disease or multiple sclerosis[29,30]. There is also research looking into the potential of manipulating the receptors to improve recovery after spinal cord injury[31].

The PARs belong to a group of seven transmembrane receptors which are connected to G-proteins, which include $G_{12/13}$, $G_{o/i}$, and G_q. The four different types of PARs differ in the composition of their N-terminal, extracellular loop 2, and C-terminal sequences. The receptor is activated enzymatically via proteolysis and this process is mediated by serine proteases[32,33]. The proteolysis process specifically cleaves the extracellular N-terminus via hydrolysis, leaving a ligand that then acts as the activator when it interacts with the second extracellular loop of the receptor. At times these receptors can also be activated by peptide sequences that are derived from the N-terminus; when there is an absence in the N-terminus cleaving mechanism, this process is another way for the receptor to be activated. There are many resulting cellular pathways that are induced by PAR activation, which include an increase in intracellular Ca^{2+},[28] tyrosine/ MAP kinase, Rho kinase, as well as phosphoinositide hydrolysis[34], and neuronal degeneration. These

pathways are activated by various G-protein subunits, which are connected to the protease activated receptors.

PAR Activators

One common activator of these PARs is the serine protease thrombin, where it plays a crucial role in the coagulation process[34]. The coagulation complex process begins when histones are released into the extracellular space by dying cells[35,36]. The histones recruit platelets to the site which then produces a quick burst of thrombin production. Thrombin interacts with thrombomodulin receptors located on endothelial cells near the injury[37]. This interaction begins a cascade that leads to more recruitment of platelets and induces fibrinogen to become interlinked fibrin in order to form a clot at the site of injury.

If neurons are near the site of injury, they could have unintended consequences induced to them due to this coagulation cascade sequence. From this information we can extrapolate that there would be harmful effects towards neurons when exposed to this serine protease. Previously it has been demonstrated when mouse neuroblastoma cells are exposed to thrombin, neurite retraction occurs[38]. There have been other experiments on primary neuronal cells *in vitro*, where they exhibited evidence of neurite outgrowth inhibition when exposed to thrombin, as well as cell death[39]. When glial cells were exposed, neurite expansion was stunted, and similarly to the neuronal cells the glial cells also exhibited cell death. The detrimental effects of thrombin were also demonstrated by the same researchers on embryonic chick spinal motor neurons, giving similar results. The cell death was deterred when the cells were exposed to the thrombin inhibitor, hirudin.

With the knowledge of the detrimental effects of thrombin, and that thrombin is a serine protease, we can further explore its role with the protease activated receptors. It has been previously reported that one specific consequence of PAR1 activation is an exacerbated amount of neuronal damage[27]. These researchers also stated that this neuronal injury was reliant on NMDA receptors. This fact is corroborated by data that the detrimental effects of PAR1 activation relies on NMDA receptor activation[40]. Further, it has been shown that PARs encouraged glutamate release from astrocytes, which is an activator for the NMDA receptors[41]. It is also important to note that in a detailed description of the mechanisms surrounding secondary neuronal cell death after brain injuries, there has

been research showing glutamate-induced neurotoxicity as a method of neuronal damage and death, with NMDA receptor activation being an important component[42]. This data leads us to understand that NMDA has an important role in the detrimental downstream effects of protease activated receptors, and thusly the thrombin coagulation complex as a whole.

PAR Inhibition

There is also evidence to allude PAR-1 inhibition also leads to a higher number of neural stem cells. It has been demonstrated that in PAR-1 knockout cells there is nearly a two-fold increase in proliferation of neural stem cells *in vitro* when compared to PAR-1+/+ neural stem cells; similar results were obtained when PAR-1+/+ neural stem cells were cultured with a PAR-1 inhibitor[43]. There was also a statistical difference in the number of neural stem cells in the subventricular zone of the brain in PAR-1 knockout mice when compared to PAR-1+/+ mice. Researchers also demonstrated positive recovery effects in PAR-1 and PAR-2 knockout mice after compression-spinal cord injury[44]. There was an improvement in the neurobehavioral locomotor recovery and less injury-related cell death in the spinal cord of these mice compared to PAR-1+/+ and PAR-2+/+ type mice. The researchers hypothesized that the reduction of neurocan they noticed in PAR-1-/- and PAR-2-/- mice directly related to the improvement in recovery. This is significant since neurocan is a known inhibitor to neurite outgrowth[44]. This information could be utilized to find the role these PARs play outside of the thrombin-induced coagulation complex, specifically in relation to PARs role in neurite growth.

It is hypothesized that inhibition of PARs could enhance neurite outgrowth in neural stem cells *in vitro,* and possibly neuronal growth *in vivo.* Serine protease inhibition may also be another way to indirectly inhibit the PARs, since they are the key activator, however NMDA-receptor inhibition could also be a target for inhibition, since there is evidence to show that PAR-induced neuronal degeneration is reliant on NMDA-receptor activation in instances of injury. Finding effective inhibitors in this neuronal degenerative cascade sequence could be the key to finding enhancements in neuronal growth *in vitro.*

Automated Analysis

Utilizing the Tecan Fluent laboratory automation workstation we can perform a screen that can quantify the quality of neurite outgrowth of cells exposed to potential inhibitors of the PAR receptor cascade. Automation of imaging allows for daily quantification of neurite growth, allowing for comparison between cells exposed to these inhibitors and the controls. The neurons that are used in the drug screen can be differentiated from hiPSCs and cryopreserved via the Tecan Fluent laboratory automation workstation. This would allow for an end-to-end process using multiple induced pluripotent stem cell lines completed with a high throughput screening experiment utilizing neurons differentiated from the iPSCs.

Overview

The goals for this project are to completely automate the maintenance process for culturing iPS cells; this includes media exchange, imaging, passaging, plating, and cryopreservation. Further, demonstrating the ability to perform a differentiation protocol, utilizing the resulting differentiated cells within a drug screen, along with automating the subsequent analysis would alleviate the amount of work that a technician is responsible for.

Materials and Methods

Human Induced Pluripotent Stem Cell Lines

There were three different human induced pluripotent stem cell (iPSC) lines used within this study. iPSC lines UMN PCBC16-iPS (lab designation UMN9-1) and 6B4 were generated and characterized as previously described (Zhang et al, 2013) (Geng et al, 2017) The hiPSC line ACS 1024 is a commercially available iPSC line (ATCC -BYS0110).

Tecan Fluent 780 Laboratory Automation Workstation

The Tecan Fluent 780 workstation provides a controlled environment with HEPA filtered laminar air flow. The Liconic incubator module was set at 37° C with a CO_2 level of 5%. The Torrey Pines heating/ cooling element is able to be set at 4°C to keep the media cooled. In order to analyze cell confluences, we used the integrated BioTek Cytation One imager using the Gen5 software. The BioTek Cytation One is an automated brightfield and fluorescence cell imager with an additional controller for temperature and CO_2 level.

Colony Imaging

The entire well was photographed every day with a 4x objective; these photos were automatically analyzed by the Gen5 software which reports a percentage of well coverage. The high-contrast imaging uses defined intensity levels to distinguish the cells from the background. The size threshold parameters are set with a minimum object size of 5µm and a maximum of 20µm, which then draws masks over the cells, which allows for proper cell counting or confluence reading.

Automated iPSC Maintenance Culture

In order to maintain iPS cell lines, there are protocols that must be executed to keep them monitored and viable, including media exchange, well imaging, and passaging. The protocols that are described here have been translated into scripts on the Tecan FluentControl software.

To assess the status of each plate, the Tecan Fluent sends a plate from the Liconic incubator, which then allows the RGA arm equipped with the eccentric fingers to transfer

the plate to the tilt carrier where it regrips the plate to transfer it to the BioTek Cytation 1 cell imaging reader. The script then directs a preset Gen5 confluency protocol to image the well. This protocol within the Gen5 software analyzes the images taken and exports an excel file with the resulting confluence of each well. When cells reached 30-40% confluency the cells were passaged onto new plates or they were prepared for cryopreservation.

Automated iPSC Media Exchange

To properly exchange media the Tecan Fluent retrieves a designated 6-well plate from the Liconic incubator and moves it to the tilt carrier by using the RGA arm accompanied by the eccentric fingers. From here, the plate cover and the media trough cover were relocated to the hotel, which allows for temporary storage and expands otherwise limited real estate within the worktable area. The tilt carrier is directed to be set at an angle of -5°, which allows the media in the plate to pool towards one side. The FCA pipetting arm then retrieves five 1000uL filtered SBS tips (Tecan 30057817), three of which are designated for removing media, while the other two are assigned to delivering fresh media. The FCA arm then aspirates 2mL of TeSR E8 media (Stemcell Technologies 05990). The FCA arm is directed to move to the plate, which then executes an aspiration liquid handling function via the FCA arm that was created to specifically remove the media from the lowest area in the plate. Since the A1 and B1 wells are in the same z-axis height, these wells are designated as ‘compartment 2’, while A2 and B2 wells are labeled ‘compartment 3’, and A3 and B3 wells are ‘compartment 4’; each compartment is designated a specific aspirating height. The ‘compartment 1’ label is reserved for aspirating from any other normal containers, referencing the ‘z-dispense’ height level for that container. After aspiration of the depleted media, the fresh media is then dispensed into the well. The aspiration of depleted media and dispensing of fresh media functions are performed one well at a time, set on a loop, with the number of loops set to a changeable variable dependent on the user’s prior input. The tips are then disposed after the plate has been completed. The lids to the plate and media trough are put back in place and the tilt carrier shakes back and forth to fully distribute the media throughout the wells. The tilt carrier is then set to 0°, which allows the RGA arm to move the plate to the transport

position, which is then placed into the incubator. This process can be repeated within the script for a specified amount of plates by activating or disabling the specific commands that designate the number of plates. The variables for number of wells designated to each plate number is easily changed at the beginning of a script; this allows for custom media exchange functions for each day, simply by running the program.

Automated iPSC Passaging

Before any passaging can occur, a 6-well plate (USA Scientific CC7682-7506) needs to be coated for the cells to be seeded onto. The plate could be prepared manually or by the Tecan Fluent, and it is coated with recombinant human vitronectin (Peprotech AF-140-09). The prepared aliquot of vitronectin stock is diluted 1:100 into $DPSB^{+/+}$ (Gibco 14040-182), distributed on the plate (1mL/ well in a 6-well plate), and incubated for at least 1 hour. Similar to the media exchange script, the Tecan Fluent will move the plate lid, aspirate 1mL of the diluted vitronectin solution, then dispense into each well. The RGA arm will then replace the lid and transport into the Liconic incubator until needed.

The passaging process runs similarly to the media exchange scripts, specifically in regard to transporting the plates and pipetting functions. The script follows the expansion protocol established in (Parr et al., 2015)[6]. The difference with the passaging script used is that at the start of the script there must be a pre-coated plate in the first position of the tilt carrier. This can easily be coordinated by withdrawing a plate that was prepared via the Tecan Fluent, or simply set into the worktable when a manual preparation was performed. This passaging script passages either one or two wells at one time. Akin to the media exchange script, a designated plate is retrieved from the incubator and placed onto the tilt carrier, where the lid is removed by the RGA arm. The tilt carrier moves to an angle of -5°. The RGA arm then drops the eccentric fingers and instead equips the tube gripper fingers; the lid to the 100mL trough of $DPBS^{-/-}$ (Life Technologies 14040-133) is removed. The FCA arm picks up 8 1000uL filtered SBS tips. Half are used to aspirate 4mL of the $DPBS^{-/-}$, and then the other half is used to aspirate the media from the wells. The FCA arm then dispenses the used media into the liquid waste trough and discards the tips. The lid to the $DPBS^{-/-}$ was put back, while the lid to the 100mL trough of hypertonic citrate solution was then removed. The solution consists of 4.4g of Sodium citrate (Sigma W302600) and

25g potassium chloride (Sigma P9333) in 1L of cell culture-grade water, and when cells are exposed to it, the solution gently detaches the iPSCs for passaging. The FCA arm retrieves 8 1000uL filtered SBS tips, using half of them to aspirate 4mL of the hypertonic citrate solution, and then the other half to aspirate the $DPBS^{-/-}$ from the wells. 1mL of hypertonic citrate solution is dispensed into each of the wells and the tilt carrier shakes back and forth to coat the entire well. The media that was aspirated is discarded into the allocated liquid waste trough. Immediately after, the solution is aspirated from the wells, and another 1mL of fresh hypertonic citrate solution is deposited onto the well. After rocking the plate, the lid is replaced, and the plate is transported into the incubator for six minutes and the pipette tips are discarded. During the incubation time, the other plate that is out on the worktable has its vitronectin aspirated and discarded, replicating the aspiration process. Dispensing 1mL of media into each of the wells follows.

Once the timer within the script reaches the six-minute mark, the plate is recalled from the incubator. At this point the hypertonic citrate solution has detached the cells. To collect the cells, two 1000uL filtered wide bore SBS tips (Tecan 30115239) are attached to the FCA arm. Once the RGA arm has removed the lid, the tilt carrier is angled, and aspiration via the FCA arm ensues. This aspiration uses a specifically designed liquid handling class labeled ‘iPSC Breakup’ that has a microscript designated to aspirate and dispense twelve times before aspirating from the lowest point of the well. Before dispensing, the RGA arm drops the eccentric fingers and equips the tube gripper fingers. It then removes a lid from a 15mL tube and transfers it to another tube in the tube rack; the cell mixture is then dispensed into the 15mL tube. Two clean 1000uL filtered SBS tips on the FCA arm aspirates and dispenses 1mL of media into each of the wells, washing them out using a modified version of the ‘iPSC Breakup’ liquid class and the wide bore tips; this modified version has half the amount of aspirations and dispenses than the normal version. That media is then aspirated and deposited into the 15mL tube. Three additional milliliters of media are also added into the 15mL tube.

In the tube rack, the first position holds a tube that contains our cell mixture, the next position holds a counterweighted 15mL tube, while the third position is an empty tube that acts as a temporary hold for the cell mixture tube lid. These tubes are moved with the RGA arm and the tube gripper fingers. The cell mixture tube and the counterweight are

moved into the below-deck centrifuge, set in opposing positions, and centrifuged at 800xg for three minutes. After the pellet is formed, the tubes are put back into place on the tube rack. The lid is also removed and placed on the empty tube. With 1000uL filtered SBS tips, the FCA arm removes the supernatant from the 15mL tube by aspirating 5.5mL and discards the media in the liquid discard trough, as well as having the tips discarded. After equipping new tips (six standard and one wide bore), 6mL of media is added onto the cell pellet. First, 1mL is added, then the wide bore tip mixes three times to disrupt the pellet. This is followed by an additional 2mL, where the same mixing process is repeated, and finally once more when the last 3mL are added. At this point, the cell pellet should be fully distributed throughout the media. The wide bore tip then aspirates 1mL of the cell mixture and distributes it into each of the wells on the new plate; this process is set on a loop dependent on the number of new wells the user has designated. The split ratio for this script is 1:3 in this setting, however there is an option to change this to a custom split ratio, as long as the ratio is in whole number integers. To finish, the tips are discarded, the RGA arm drops the tube gripper fingers and reequips the eccentric fingers to put the lids back onto the plates and the media trough. The new plate is moved onto the transport position, but before being inserted into the incubator, the RGA arm lifts and shakes the plate three times in the x-direction, twice in the y-direction, then twice more in the x-direction again. The rest of the worktable is then cleared manually for the next script.

Automated iPSC using ReLeSR Passaging

The passaging was also performed using the reagent ReLeSR (Stemcell Technologies 05872) as a passaging reagent instead of the hypertonic citrate solution. With this protocol, the steps are nearly identical, however with this reagent centrifugation is unnecessary. Following the normal passaging script, once the media is aspirated from the plate via the FCA arm, 1mL of ReLeSR is added to each of the two wells. A timer starts immediately after, then the tilt carrier shakes to coat the entire well. Once the timer reaches 25 seconds, the FCA arm aspirates the ReLeSR from the plate and dispenses it into the liquid waste container, leaving a film of ReLeSR coating the cells. The RGA arm then replaces the lids and moves the plate for incubation for 4.5 minutes. 1mL of media is added to the wells once the place is properly moved back onto the tilt carrier and the lid has been

removed. At this point, there has to be manual intervention to shake the plate, since the Tecan Fluent cannot contribute enough shear force to the plate to dislodge the cells. A simple aspiration at an angle is enough to collect the cells with the wide bore tips, where it can be collected into a 15mL tube. Equivalently to the post supernatant aspiration, the cell mixture is diluted to 6mL with intermittent mixing and distributed amongst the wells on the new plate.

Automated Cryopreservation Preparation

The cryopreservation protocol utilizes the ReLeSR passaging script that was previously described to disassociate the cells, with some changes. Once the plate is removed from the incubator and placed onto the tilt carrier with its lid removed, then 750mL of a basal solution containing poloxamer 188 (P188; NF grade; Spectrum Chemical) is added into the two wells. 500uL of the solution is also added into a designated dummy cryovial. The poloxamer 188 works as a copolymer with the proprietary DMSO-free cryopreservation reagents that improve cryopreservation properties. Manual shaking of the plate occurs, then the lid is removed again followed by aspiration of the cell mixture. Similar to the passaging script, they are collected in a 15mL tube with 1000uL wide bore tips, however no media is added to dilute the cells. Instead of distribution throughout wells on a new plate, 500uL the cells are instead dispensed into cryovials that are aligned in a cryovial rack runner in the worktable. With the tips discarded, a single new 1000uL tip is equipped to slowly, dropwise, add 500uL non-DMSO cryoprotective agents (USP grade; Sigma-Aldrich, Humco, Grifols, Spectrum Chemical) to each of the cryovials, including the dummy vial. The script is then finished, and manual intervention must ensue.

With the lids on the cryovials loosely capped, 1 hour of room temperature incubation occurs. 15 minutes before the hour timer has ended, a separate controlled-rate freezer is booted and calibrates to room temperature with the dummy vial connected to the sample temperature probe. When the timer ends, the cryovials are manually loaded into the freezer, where the ‘hiPSC B-1 AUTO NUC-4’ controlled-rate freezer program is activated. This program was previously modified to automatically induce ice nucleation via a fast dive to -45 ˚C followed by a rapid increase in temperature to -12.4 ˚C. The program follows the directions listed here:

0. Starting temperature 20 ˚C
1. (a) -10 ˚C/min to 0 ˚C
   (b) Hold at 0 ˚C for 10 min to equilibrate temperature inside and outside vials
2. (a) -50 ˚C/min to -45 ˚C to induce ice when temperature inside vials was ~ -4 ˚C
   (b) +15 ˚C/min to -12.4 ˚C;
   (c) +2.16 ˚C/min to -7.4 ˚C to prevent temperature overshoot;
3. -1 ˚C/min to -60 ˚C;
4. -10 ˚C/min to -100 ˚C.

Once the controlled-rate freezer program has completed, the vials were transferred to liquid nitrogen for storage. The temperature of both the sample and freezer were each recorded on a print-out to confirm the program was executed properly.

Automated Wash-free cell thawing

To thaw the cells, a cryovial retrieved from the liquid nitrogen storage is manually transferred into the Biocision ThawSTAR, which quickly thaws the cells in less than 5 minutes. Equivalently to the passaging scripts, a vitronectin-coated plate has the coating aspirated and has 1mL of TeSR E8 medium dispensed into each well of the 6-well plate. This plate then has the lid replaced and is transferred to the Liconic incubator via the RGA arm for 10 minutes. During the incubation time, the cryovial is manually transferred to the cryovial rack runner with its cap removed. The FCA arm retrieves a 1000uL wide bore tip and one 1000uL tip, and then using the wide bore tip mixes once by aspirating and dispensing back the cell solution, then aspirates and collects the cell solution into a 15mL tube. 1mL of media is dispensed into the cryovial with the standard tip, where another mix and transfer to the 15mL tube occurs with the wide bore tip. The dispensing of this washed media into the 15mL tube was performed dropwise into the cell solution. With clean tips attached, the FCA arm aspirates 5mL of media to dropwise dilute the cell solution in the 15mL tube. At this point the plate is recalled from the incubator and replaced onto the tilt carrier, with its lid removed. The cell solution is mixed five times to evenly distribute the cells within the mixture, and then 1mL of the solution is dispensed in each well of the plate. The RGA arm then shakes the plate as described in the passaging script and deposits the plate into the incubator. The next day before a media exchange, the cells are washed with $DPBS^{+/+}$ before fresh media is added onto the cells. This is to ensure that any traces of the cryoprotectant are removed.

Automated Neuronal Differentiation

To start the differentiation process, iPSCs are distributed onto a 6-well plate coated with laminin (rhLaminin-521, ThermoFisher A29249). This task is able to be performed by the Tecan Fluent. Another script was written to distribute an allocation of small molecules in separate wells of a 96-well plate (USA Scientific CC7682-7596); this is so that the molecules can be integrated into a specific daily media that will be used to differentiate the cells. At the beginning of the script, the Eppendorf tube rack runner in the worktable was filled with eleven different Eppendorf tubes containing small molecules. The RGA arm removes the lid of the 96-well plate into the hotel. The FCA arm equips Tecan 50uL filtered tips (Tecan 30057811) and transfers a specified amount of each into different wells of the 96-well plate; the amounts of small molecules follow the differentiation protocol described by (Walsh et al., personal communication). The filled wells in this plate are organized by each of the six days to ease the script writing. New tips were acquired between each Eppendorf tube. Once done with the allocation, the RGA arm moves the lid back onto the plate and the Torrey Pines heating/ cooling element is set to -20˚C to keep the molecules frozen.

Each day of this six-day protocol requires a media exchange that uses a media that is created within that script. Essential 6 Medium (ThermoFisher Scientific A1516401) was used as the base to the daily media that was created. Before the standard steps that were previously described to perform the media exchange, the RGA arm removed the lid to the media trough that contains the Essential 6 Medium. With 1000uL tips equipped, 14mL of media is transferred from the media trough to an empty 100mL trough. At this point the RGA arm removes the lid from the 96-well plate containing the stock molecules. 100uL of the media is transferred to each of the wells specified for that day. A mix occurs, then an aspiration of 100uL plus the volume of small molecules in the well is used to transfer all of the well contents back into the 100mL trough. This happens once more to fully wash out the well. From here, the steps in the script follow the media exchange script with this newly created media. After six days the differentiation of the iPSCs into neurons would have occurred. These neurons can be passaged and frozen for future use by using the previously stated cryopreservation script.

PAR Inhibitor Drug Screen Set-up

To set up the PAR inhibitor experiment, a 96-well plate coated with laminin is seeded with neurons that were frozen as previously described. A script has been created to follow the previous thaw script, however it has been modified to distribute onto a 96-well plate. The final diluted concentration of the frozen neurons was aimed to be around 2,000 cells per well; this dilution calculation was performed with a hemocytometer. To ensure proper homogeneity within the solution, a gentle mix step would occur after every other aspiration. A 1000uL wide bore tip would aspirate a 400uL to allocate 100uL to four wells at a time, starting with well A1 to D1, followed by E1 to H1, then moving onto the next column. These short distributions were necessary to ensure equal seeding densities between the wells. After seeding, the cells are able introduced to a varying amount of concentrations of the drugs listed in Table 1, ranging from 0.001uM to 100uM diluted in a basal media:

Table 1:

Compound	Manufacturer	Catalog #
Methyl Mercury	Millipore Sigma	442534-5G-A
Dieldrin	Millipore Sigma	33491-100MG-R
Rotenone	Millipore Sigma	45656-250MG
Valproic Acid	Millipore Sigma	PHR1061
Antimycin A, Antibiotic	Abcam	ab141904
Valinomycin	Millipore Sigma	V0627-10MG
MK-571 sodium salt hydrate	Millipore Sigma	M7571-5MG
Mitomycin C from Streptomyces caespitosus	Millipore Sigma	M4287-2MG
Staurosporine from Streptomyces sp.	Millipore Sigma	S5921-.1MG

Once plated and exposed to the compounds, the cells stay incubated for three days. On the third day the wells have their media exchanged using the half-media aspiration script to avoid damaging the neurons. One set of control cells were fixed at this point to confirm their phenotype via immunocytochemistry. After ten days the cells are fixed for immunocytochemistry. Brightfield photos of the neurons were taken daily with varying

focus levels; this was done so there would be a focused image for the neurite outgrowths and the cell bodies. The images captured by the Gen5 software can be transferred to another program called CellProfiler. This software is able to stepwise edit and enhance photos in a pipeline fashion; this allows for integrating multiple pictures of the same wells that could be used to distinguish the separation of neurites from the cell bodies. The program begins with an autofocus bright field image, setting the fusion method to linear blending, and cropping. Next, the names of the layers are defined, which allows the program to separately apply different settings. The background for all of these photos are set to dark. The program then brings in the -165µm photo; parameters are defined with a background flattening size of 20µm and 0 image smoothing strength for maximum cell body definition. The -110µm photo has its parameters defined with background flattening size of 5µm and an image smoothing strength of 3 for optimal neurite specification. The measurements are then calculated by selecting the neurite outgrowth borders, deselecting the defined areas of the cell bodies, then outputs a calculated measurement. By using this method CellProfiler is able to automatically measure the neurite outgrowths from each cell.

Immunocytochemistry and Automated Quantitative Microscopy

There are several instances of immunofluorescence within these experiments, and they are detailed in the antibody table (Table 2). To begin, cells were fixed by adding 1mL 3.7% formaldehyde (Sigma-Aldrich) for 10 minutes at room temperature, followed by a wash with $DPBS^{-/-}$. To permeabilize, 0.2% v/v Triton X-100 (Sigma-Aldrich) in $DPBS^{-/-}$ was added, and then blocked with blocking buffer (1% BSA (Sigma-Aldrich), 0.1%v/v Tween20 in PBS). Primary antibodies (Table 2) were added after being diluted in blocking buffer, which was then incubated overnight in a refrigerator to keep at 4˚C. Secondary antibodies (Table 2) were also diluted in blocking buffer and incubated at room temperature for 2 hours. DAPI (Roche) was diluted 1/1000 in $DPBS^{-/-}$ and added to create a nuclear counterstain. Fluorescent images were taken by using the Cytation One cell imager with a 20X objective in manual mode with auto-focus and auto-exposure.

Table 2:

Antigen	Host	Brand	Catalog #	Dilution ratio
iPSC Antibodies				
OCT4	Mouse	Millipore	MAB4401	1:250
NANOG	Goat	R&D Systems	AF1997	1:100
Tra-1-81	Mouse	Millipore	MAB4381	1:100
Neuron Antibodies				
4G11-s Engrailed-1	Mouse	DSHB	N/A	1:20
FoxP2	Rabbit	Novus Biologicals	NBP2-30063	1:20
Isl1	Mouse	DSHB	PCRP-ISL1-1A9-S	1:250
Alcam	Mouse	R&D Systems	MAB6561	1:200
Nurr1	Goat	R&D Systems	AF2156	1:100
MAP2	Rabbit	Millipore	Ab5622	1:1000
Synaptophysin 1	Guinea Pig	Synaptic Systems	101 004	1:1000
Gad67	Mouse	Abcam	ab26116	1:100
GAT1	Rabbit	Abcam	ab64645	1:500
ChAT	Sheep	Abcam	ab18736	1:1000
Glutamate Synthetase	Mouse	BD Transduction Laboratories	610517	1:500
β-III-Tubulin	Mouse	Abcam	Ab7751	1:500
Secondary Antibodies				
488 – Donkey Anti-Mouse		ThermoFisher Scientific	A-21202	1:500
555 – Donkey Anti-Rabbit		ThermoFisher Scientific	A-31572	1:500
555 – Donkey Anti-Goat		ThermoFisher Scientific	A-21432	1:500
555 – Goat Anti-Guinea Pig		ThermoFisher Scientific	A-21435	1:500
555 – Donkey Anti-Sheep		ThermoFisher Scientific	A-21436	1:500
647 – Donkey Anti-Rabbit		ThermoFisher Scientific	A-31573	1:500

Results

Cryopreservation & Thawing

To extend the capabilities of the UMN Workstations, scripts for cryopreservation and post-thaw plating of cells were written and implemented on the UMN Tecan Fluent 780 platforms. The cryopreservation script was performed using the laboratory 9-1 iPSC line. To test whether the automated cryopreservation script successfully preserved the cells, the thaw and plating script was performed to distribute cells onto 2 wells of a 6-well plate. Figure 3A-D shows the results of this initial plating, with well A1 being passaged after

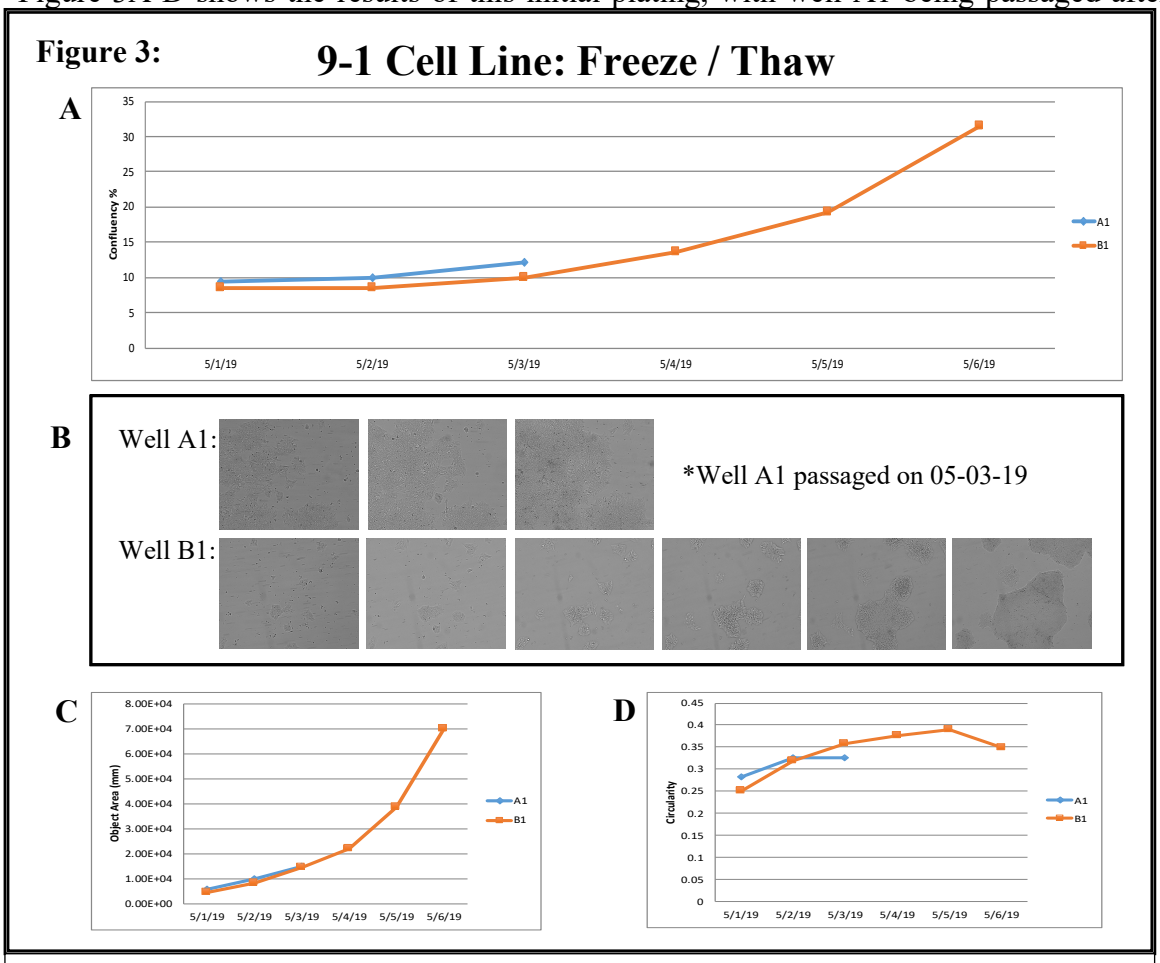

Figure 3: This figure shows the results from the 9-1 iPSCs that were thawed and plated via the Tecan Fluent 780. The cells were thawed 4 days after initial freezing. Initial analyses were performed 1 day after plating. (A): The confluency percentages of the thawed 9-1 cells. (B): Representative images of the wells for each day cultured. All images in each row correspond with the dates of analysis. (C): The total object area for each well over the time period. (D): The circularity of the cells over the specified dates are shown.

three days of culture, and well B1 being passaged after 6 days. Each day during the specified growth period images and measurements were taken of the cells, then the media was changed. This process was performed entirely using the automated scripts. The confluency over this time period is presented in Figure 3A, with representative images of the growth shown in Figure 3B. The change in object area and object circularity are shown in 3C-D respectively. The object area provides a quantitative measure confirming the confluency measurement. Object circularity is observed, since the general morphology of iPSC colonies are mostly uniform. It has been noticed in our research that as the iPSC colonies become denser and may merge, the circularity measure decreases. A dramatic decrease to close to 0 in circularity can be noticed if colonies exhibit differentiation.

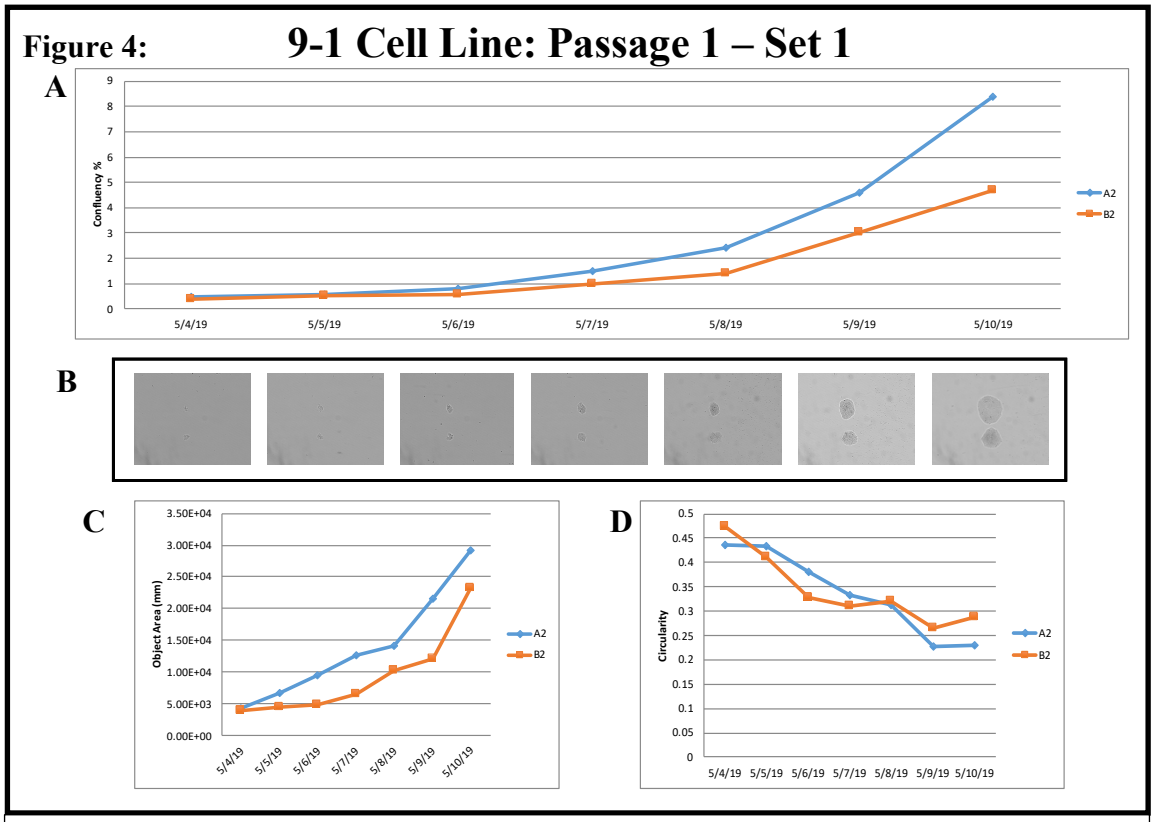

Figure 4: This figure shows the results from the first passage of the 9-1 iPSCs that were thawed and plated via the Tecan Fluent 780. The cells were passaged and plated after 3 days of culture. Initial analyses were performed 1 day after plating. (A): The confluency percentages of the passaged 9-1 cells. (B): Representative images of the wells for each day cultured. All images in each row correspond with the dates of analysis. (C): The total object area for each well over the time period. (D): The circularity of the cells over the specified dates are shown.

After three days well A1 was passaged due to high regional confluency. This was likely due to having an insufficient shake step incorporated into the initial plating script and an improved plate shaking step was implemented in all future scripts. After six days the B1 well was passaged after reaching 30% confluence. Passaging was performed utilizing the automated passaging script. The results of the first passage are shown in Figure 4A-D, showing a low initial density, but with a standard recovery rate. The split ratio for this passage script was set to a 1:6 ratio. Initial density is quite lower than expected with the low split ratio. Script changes were made after these results were obtained so an option is available to incorporate a custom split ratio. Even with the custom split ratio option, the resulting density after passaging varied greatly in future script executions depending on how well the automated protocol was executed.

Three passages were performed in total, which resulted in ten separate growth curves. The accumulation of the confluency data can be seen in Figure 5A. More detailed data from each of these passages can be found in Supplemental Figures 1-3. Figure 5B shows the hierarchy of the passage lineage, and from which well each originated from. The confluency rate is quite consistent throughout the passages, however since the split ratio was programmed at a 1:6 ratio, the initial confluence is not ideal. It would have been preferable to begin above 5% confluency. Even with the low initial confluency, cell recovery after cryopreservation has been demonstrated, as well as the ability for the cell maintenance and data collection protocols to be automated.

To test if the iPSCs retained their inherent phenotype characteristics, differentiation and immunohistochemistry was performed on cells post-thaw. To accomplish this, additional frozen 9-1 iPSCs were thawed and plated onto three separate 6-well plates. One plate would be dedicated to a tri-lineage differentiation, one to neuronal differentiation, and one to OCT-4 and NANOG immunohistochemistry. Figure 6 shows a successful recovery from cryopreservation before tri-lineage differentiation was performed. Figure 7 contains similar successful data after cryopreservation, as well as some of the resulting representative images of the differentiation process. It was noticed during this process that a high proliferation rate was still present throughout the process. Due to this, the conditions for proper immunohistohemistry are less than ideal. Further, the measurements taken

Figure 5:

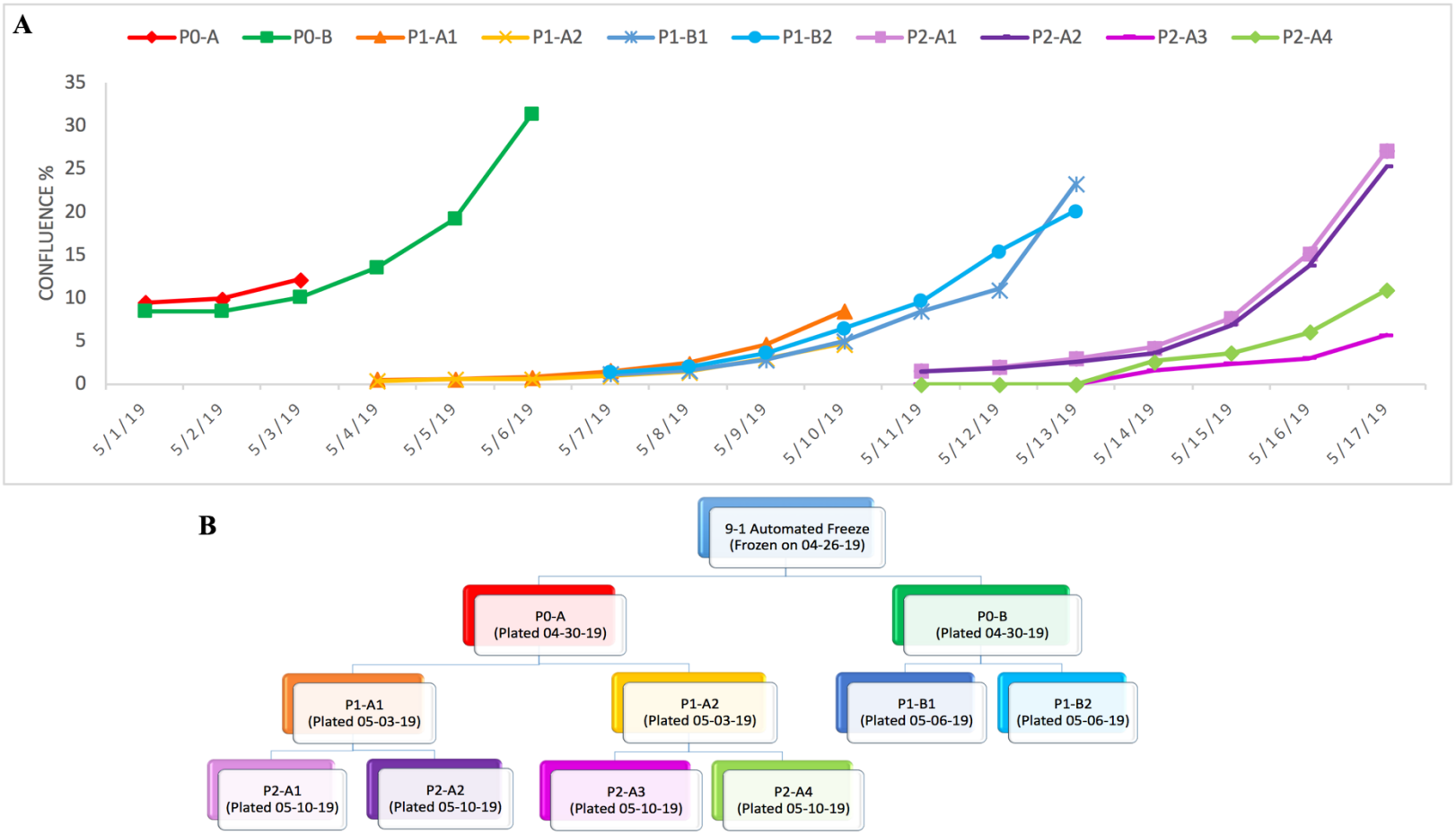

Figure 5: This Figure represents three passage generations of the DMSO-free automated freeze 9-1 cell line. (A): This graph depicts the confluency for each specific well, with passages occurring when the series has terminated. (B): A hierarchy showing the lineage of the collected data.

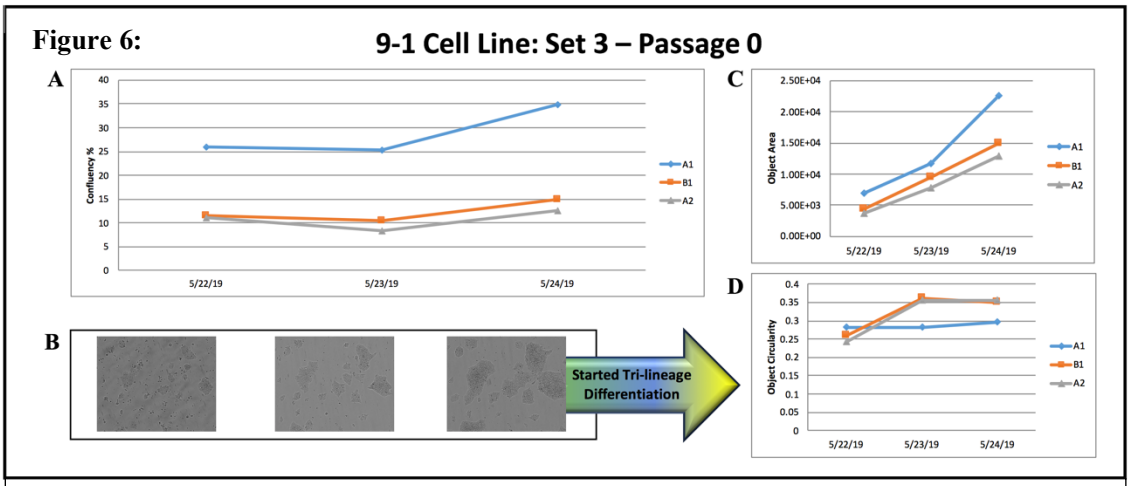

Figure 6: This figure shows the 9-1 iPSCs that were thawed and plated via the Tecan Fluent 780, which will go onto Tri-Lineage differentiation. The cells were thawed 21 days after initial freezing. Initial analyses were performed 1 day after plating. (A): The confluency percentages of the thawed 9-1 cells. (B): Representative images of the wells for each day cultured. All images in each row correspond with the dates of analysis. (C): The total object area for each well over the time period. (D): The circularity of the cells over the specified

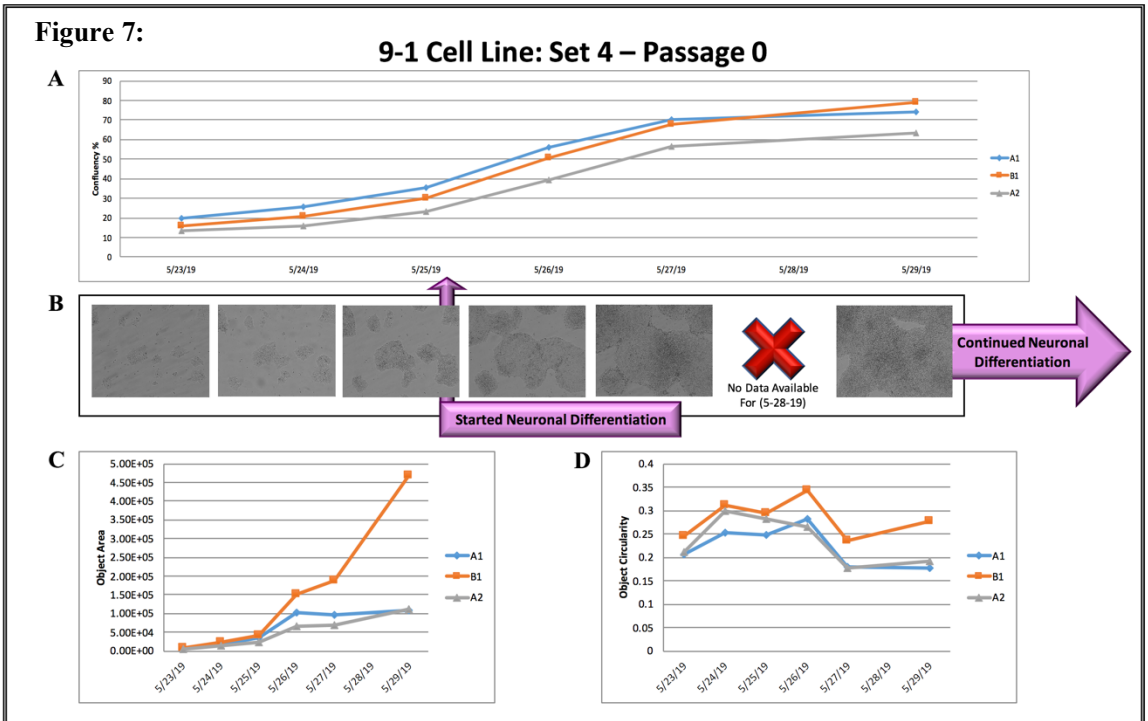

Figure 7: This figure shows the 9-1 iPSCs that were thawed and plated via the Tecan Fluent 780, which will go onto Neuronal differentiation. The cells were thawed 21 days after initial freezing. Initial analyses were performed 1 day after plating. (A): The confluency percentages of the thawed 9-1 cells. (B): Representative images of the wells for each day cultured. All images in each row correspond with the dates of analysis. (C): The total object area for each well over the time period. (D): The circularity of the cells over the specified dates are shown.

during the final experiment were unavailable due to an error. Because of these issues the neurons were passaged and frozen manually using a DMSO cryopreservation solution. Subsequent attempts to thaw and plate the neurons were unsuccessful. The OCT-4 and NANOG antibody detection was performed, however poor results were captured, likely due to a failure in the immunofluorescent staining procedure execution. Repeating this in the future will be necessary to determine if the cells have retained their pluripotency characteristics.

Automated Neuronal Cell Screen Set-up

One goal of this research for translating manual stem cell differentiation protocols to an automated version. This work will be incorporated into a drug screening protocol utilizing iPSC-derived neurons in a 96-well plate format to test the effects of various drugs on growth and differentiation over a time course of a few days. In order to prepare for the drug screen process, a critical factor to account for is consistent numbers of cells plated in each wells. This is to ensure there are no significant differences present between wells, which could change results in drug presence per cell or even general cell maintenance during the process. In preliminary work a density of around 2000 cells per well was found to be a cell concentration that allowed proper automated neurite outgrowth analysis with the automated imaging. These tests were the first scripts created, so perfect execution was not expected initially.

The first experiment was to test the distribution script set up to see how evenly the cell numbers are between all of the wells. The first two trials utilized iPSCs from frozen stocks. Using iPSCs at this point was not detrimental for testing the distribution of cells, since this is just the preliminary tests for even cell delivery. The initial script setup follows a script comparable to the final Thawing & Cell Distribution script. The most discrepancies between the initial script and the final script for this protocol dealt with the transfer of cells from the 15mL tube to the 96-well plate. Each well in the 96-well format is filled with 125µL of media, therefore 1mL of media can be distributed amongst 8 wells. Because of this, the initial script would use one 1000µL wide bore tip to aspirate 1mL of the cell solution. An initial mixing step would take place beforehand, mixing the solution three separate times. After every other cell solution aspiration, a following mixing step would

occur. The aspiration task for this first test used a simple liquid class Fluent control script element labelled “Media”, which uses 100% speed and aspirated a few millimeters below the top of the liquid using the liquid level detection. The cell solution would then be dispensed 125µL at a time into all eight wells in a column.

Figure 8A and 8B showcases the initial distribution script test results. Figure 8A shows the average confluency percentage, which is just under 11%. The standard deviation for this test run is incredibly high at 81%. The high variability between wells is better demonstrated in Figure 8B, which states the confluency for all 96 wells and is formatted to

Figure 8:

A

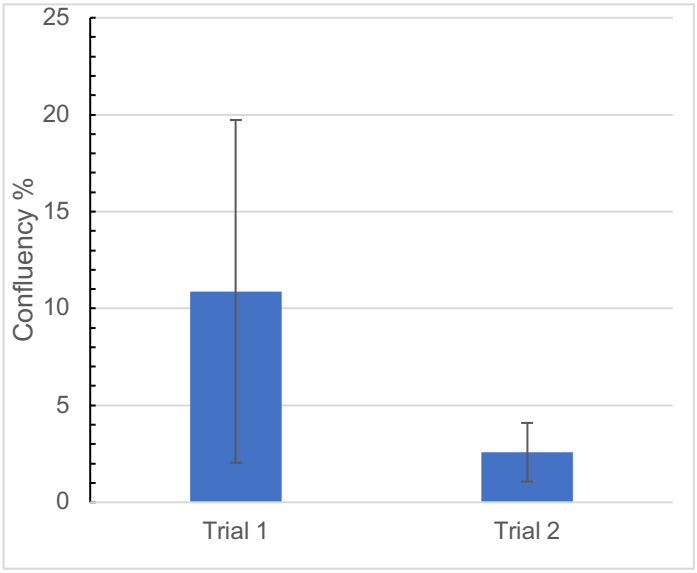

B

14.368	24.053	24.235	31.308	17.585	16.04	16.63	13.605	1.847	0.63	0	0
27.419	29.166	21.394	10.007	15.715	20.126	12.135	6.885	7.832	0.01	0	0
16.123	24.159	12.743	13.896	11.251	13.248	20.793	11.773	11.108	0	0	0
7.599	15.547	31.31	21.214	25.514	20.99	22.976	13.502	21.833	0	0	0
9.869	27.2	21.676	11.756	16.292	25.079	8.515	16.773	19.099	0.092	0	0
18.214	15.384	19.465	13.123	16.522	15.909	15.182	9.337	4.753	0	0	0
7.511	6.568	12.505	6.128	7.698	11.149	8.825	8.581	3.675	0.039	0.051	0.01
4.005	6.208	10.336	6.553	9.528	7.004	7.434	6.265	3.73	0	0	0.012

C

6.87	0.959	2.182	1.91	1.404	0.928	1.582	2.048	1.1	2.535	1.756	1.236
6.497	1.747	2.252	2.725	5.775	3.361	2.608	4.201	3.14	1.655	2.986	3.153
7.641	4.13	2.42	3.962	2.692	2.891	2.092	3.05	2.208	2.118	0.66	0.704
7.443	3.202	2.87	1.956	2.718	2.367	2.192	3.144	1.342	1.889	2.063	1.179
4.307	1.661	1.391	2.641	1.294	3.874	2.395	3.194	2.357	1.415	1.456	2.523
4.248	3.649	1.743	2.641	1.957	4.819	3.662	2.843	2.012	1.709	2.492	2.037
1.55	1.405	3.329	1.937	1.951	2.285	2.325	2.689	2.525	3.091	1.962	1.903
9.254	1.734	1.732	1.988	2.105	1.404	1.668	0.751	0.856	1.704	1.444	2.312

Figure 8: The results from the first two iPSC distribution trials throughout a 96-well plate. (1A) shows a graph depicting the average confluency percentages with error bars reflecting the correlating standard deviation. Trial 1 had a confluency of 10.8% and a SD of 81%, while Trial 2 had a confluency of 2.6% and a SD of 59%. (1B, 1C) shows the confluency per well in the 96-well plates of each trial, with white cells being the lowest number of cells and dark blue being the most concentrated.

emphasize high confluency with dark blue coloring and low confluency with light blue. The final three columns in the 96-well plate are zero or near zero, which indicates that too many cells have been aspirated between the first nine columns. Further, it is apparent that the bottom two rows have consistently less cells than the first six wells in every column. It was thought that the cells were concentrating at the bottom of the pipette as the pipetting was occurring, distributing most of the cells in the pipette before the last two wells. To directly address this, distribution of the cells changed from eight-at-a-time to four-at-a-time. Additionally, a mix step was added between every eight wells versus the original sixteen to ensure a more consistently homogenous solution. The cell solution concentration was also diluted to a more appropriate level.

The second trial's results are presented in Figure 8A and 8C, which shows an average confluency at just over 2.5%. Contrary to standard good practice, the vials of frozen cells were not counted before the freeze, nor once thawed, therefore there is not a proper method at this point to ensure consistent plating confluency between the trials. I did not think that would be too variable for the overall tests, since lowering the standard deviation for each trial was the goal for these trials; proper confluence could be addressed with a counting step in the future. The standard deviation shown in Figure 8A is 58%, which is an improvement on the initial script trial. There is an obvious high number of cells in the first column in Figure 8C; one hypothesis was that this was due to inadequate mixing before any distribution attempts. To fix this, an additional mix was added after every 4 wells. The aspiration location was also changed from using liquid level detection, which would aspirate near the top, to the "Z-max" location, which is near the bottom of the 15mL tube.

Following these first couple of tests with iPSCs, iPSC-derived neurons were then used once they became available. The initial concentration of cells/ cryovial was not calculated beforehand, nor was the ideal concentration in each of the wells of a 96-well plate known. It was more convenient at the time to test the latest version of the script with the new cell type; Figure 9A and 9B shows the results from that test. The average cell count was around 3,800 cells per well with a standard deviation of 18%, which is a significant improvement on the previous tests. There are fewer cells in the first column, as well as the last well in each distribution loop. In order to overcome these issues, extra mixes

beforehand were added, as well as between every other distribution to more thoroughly mix the cell solution. The script was also adjusted for lower distribution so that the number of cells would be about half. To accomplish that task, instead of diluting the cryovial to a

Figure 9:

A

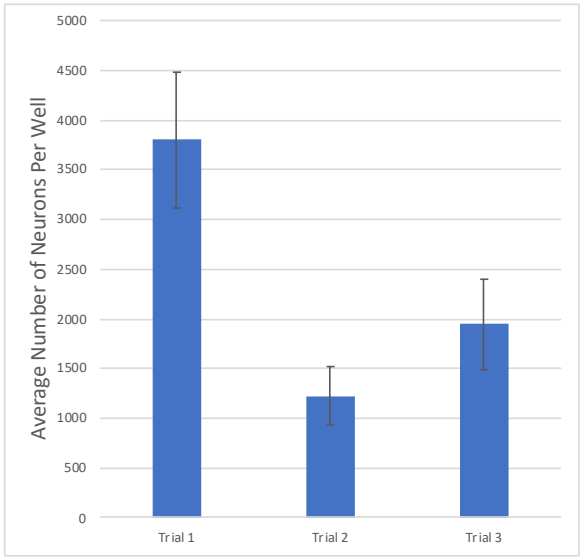

B

3031	2957	2627	2575	2732	2611	3047	3105	3458	2863	3911	3230
3357	3881	4171	3903	3957	3988	4218	3983	4182	4634	4835	3771
3207	3725	3800	4392	4542	4527	3826	3911	4547	4343	5061	3415
2766	3420	3840	3495	3458	4284	3863	4139	4091	4318	4772	3446
2783	3672	3936	3941	4893	4370	3964	3866	4524	5169	4320	3383
3033	4307	4673	4438	4191	4628	4395	4517	4786	3959	4194	3075
3106	4303	3805	3749	4790	3811	4101	4035	5051	4992	4184	3177
2766	3490	3486	3106	3292	2518	2478	2553	3405	3527	3175	2857

C

1135	1657	1127	1155	1620	1393	790	1392	1300	1501	1517	870
1653	1352	942	1538	1290	1732	1732	1589	1493	1398	1112	964
1210	1447	1770	1191	1228	1393	1162	1414	746	1005	1189	753
1386	1476	1182	1105	1103	1214	1808	661	929	1019	1048	895
1062	996	1209	1212	1406	1497	1445	1327	1159	1208	1267	779
1477	1471	1473	1526	1557	1539	1685	1353	1095	1139	873	471
1595	1208	1211	1207	1013	1292	828	1560	875	1147	881	790
1356	1152	1358	833	954	1278	1552	1332	893	1326	841	414

D

1854	2634	1712	1823	2635	2209	1205	2244	2102	2338	2378	1417
2474	2205	1459	2321	2158	2658	2734	2432	2323	2126	1776	1477
1843	2332	2738	1847	1953	2387	1848	2238	1211	1578	1841	1190
2235	2247	1877	1739	1915	1930	2951	1097	1535	1673	1617	1340
1674	1620	1888	1883	2204	2353	2190	2149	1777	1996	1977	1216
2433	2521	2292	2454	2457	2466	2554	2106	1743	1733	1356	816
2433	1904	1993	2095	1811	2103	1290	2528	1396	1896	1350	1237
2013	1920	2197	1404	1569	2059	2466	2125	1437	2107	1308	658

Figure 9: The results from three neuron distribution trials throughout the 96-well plate format. (1A) shows a graph depicting the average number of neurons with error bars reflecting the correlating standard deviation. Trial 1 had an average number of 3802 and a SD of 18%, while Trial 2 had an average number of 1226 and a SD of 24%. Trial 3 resulted with 1948 average number of cells, with a 24% SD. (1B, 1C, 1D) shows the number of cells per well in the 96-well plates of each trial, with white cells being the lowest number of cells and dark blue being the most concentrated.

full 12mL amount, 6mL of the media would be evenly added to the plate first, then the cell solution in the cryovial would be diluted to 6mL and distributed.

The second neuron plating trial results are shown in Figure 9A and 9C. The script was successful in that it was able to reduce the number of cells per well, however there was an error by the machine in that it ran out of the diluted cell solution during the distribution phase for the last 12 wells, which was likely do to a dispensing error. The resulting average is 1,226 cells per well, with a standard deviation of 24%. If the last column was omitted, since that was when the error came about, the standard deviation dropped to 20%. This indicated that a standard deviation of around 20% would be an average amount of deviation to expect between wells, which also was not detrimental to the goal since a 20% deviation did not impact the future processing steps. It was noticeable after this trial that the concentration of the neuron cells in the cryovial used for this second trial was lower compared to the first trial. Since it was unknown whether the other cryovials would contain a consistent concentration of neurons, it was necessary to add a manual cell counting step within the script to account for an even distribution between every experiment using this script. This involves having the script deliver an aliquot of the cell solution into an Eppendorf tube, then pausing the script so that it can be manually mixed with Trypan Blue and counted on a Hemocytometer. The total cell count found from that could be inputted into the script in the following step under the variable "NumCells". The equation that was used also referenced the other following variables:

$$\text{"CellMixPerWell"} = \frac{\text{"NumCellsPerWell"}}{(\frac{\text{"}NumCells\text{"}}{3mL})} * 1000(\frac{\mu L}{mL})$$

The "NumCells" variable is divided by 3mL, since that is the amount of media the cells are diluted into. The "NumCellsPerWell" is a pre-set variable and is set to 2000 cells per well. This value is then multiplied by 1000 to convert the units into microliters. The equation is then set to the "CellMixPerWell" variable, so that this amount is how much cell solution will be dispensed into each well. Simply subtracting the "CellMixPerWell" from 125µL is the amount of media that is added into each well of the 96-well plate. After integrating the equation into the script, the distribution was tested again. The results are

shown in Figure 9A and 9D. We can see that the average cell count of 1948 cells is nearly the goal of 2000, which is specified in the variable "NumCellsPerWell". The standard deviation on this data set is 24%. It is seen again in figure 9D that the cell count is towards the lower end. Without the last eight wells, the average is 2019 cells per well with a 20%, which is right on the target goal; the low amount of cells at the end may have occurred due to the minimal cell solution left in the 15mL tube, which could be solved by initially diluting the entire solution with a small addition of media.

Neuron Media Exchange

Once a proper density of neurons has been seeded onto the 96-well plate, daily media exchange would be needed to maintain them. After an initial practice run of the 96-well media exchange script it was noticed that there was some cell loss. A quick test was run to see if there are differences in using a default aspiration liquid class compared to one set to 30% aspiration speed. Comparing the standard procedure of removing all media to exchanging half the amount of media was also tested. Figure 10A&B shows that the least

Figure 10:

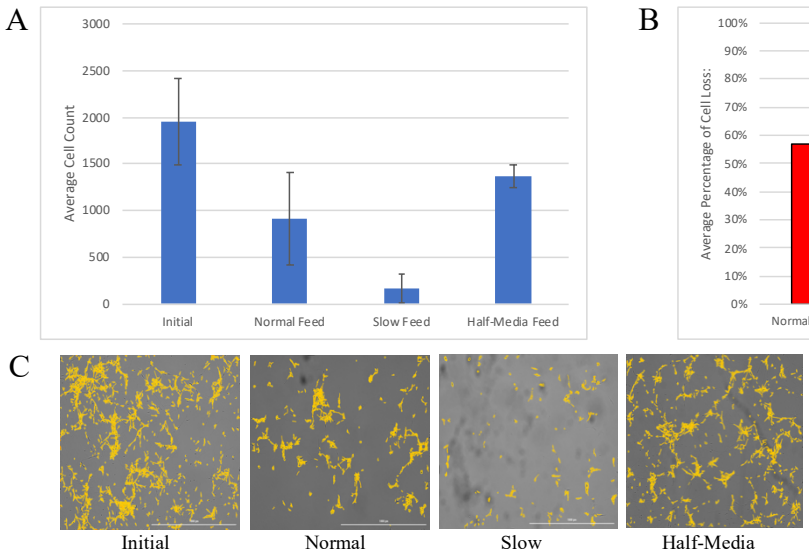

Figure 10: 96-well media exchange tests were performed using different script alterations which include default liquid class aspiration, 30% of aspiration speed, and 50% amount of media exchanged. (A): The resulting average cell counts over the wells tested. (B): The average percentage of cell loss per method used. (C): Representative photos of the wells after a specified media exchange method, with the yellow showing the Gen5 software cell outlines of the neurons.

amount of cell loss was using the half media exchange script with cell loss at only 44%. Representative photos of the gating and counting step of these media exchange analyses are shown in Figure 10C. Further tests with additional parameters are planned to further find a more efficient media exchange method to minimize cell loss.

Neuron ICC Characterization

To elucidate a more specific characterization of the neurons that were differentiated using the same method that will be implemented on this automated platform, immunocytochemistry was performed to stain for specific neuronal identifiers. This characterization would serve as a control to compare cells differentiated using an automated differentiation script. Table 2 refers to the neuronal-specific antibodies used

Figure 11:

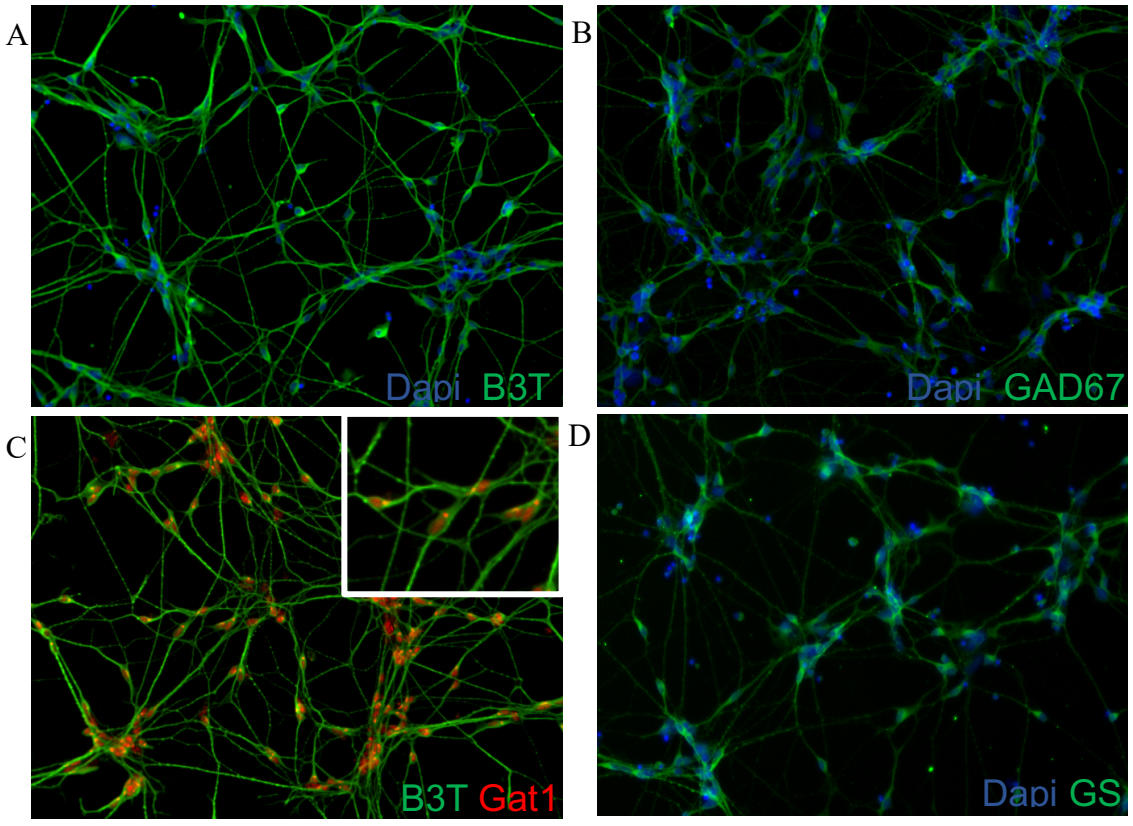

Figure 11: Immunocytochemistry of the automated-plated neurons (4A): Representative photo showing Beta-III-Tubulin staining. (4B): Representative photo showing GAD67 staining. (4C): Representative photo showing Beta-III-Tubulin and Gat1 staining. An enlarged image showing distinct regional staining. (4D): Representative photo showing GS staining.

from the selection of available antibodies. Of the many neuron antibodies listed, only a small portion of them were positive. β-III-Tubulin, Glutamate decarboxylase (GAD67), GABA Transporter 1 (GAT1), and Glutamate synthetase (GS) were successfully shown by Figure 11 to be present in the neurons plated. There is a positive expression of β-III-Tubulin as shown in Figure 11A, which is exclusive to neuron cell types. The presence of GAD67 in Figure 9B and GAT1 in Figure 11C are indications of a GABAergic interneuron phenotype. To determine a more thorough characterization, additional immunocytochemistry with more antibodies and other characterization tests would be needed to more finely define these neurons. This includes antibodies for motor neurons, such as Isl1 and HB9, the maturity antibody MAP2, and neuron subtype antibodies such as GATA-3 and Sim1.

Neurite Outgrowth Imaging

In order to analyze the effects that various drugs have on the neurons, measuring the neurite outgrowths in an automated and efficient manner is critical. It is important for this experiment to continually monitor the outgrowth levels at different time points to determine the effects over several periods of time. This can allow us to determine how long each concentration of drug reacts with the neurons, giving us a time point measurement for rate of effect. The only previously established method for automated neurite outgrowth limits the analysis portion to one time, since it requires fluorescent staining. With the automated imaging already in place, using the images obtained from the Gen5 software

Figure 12:

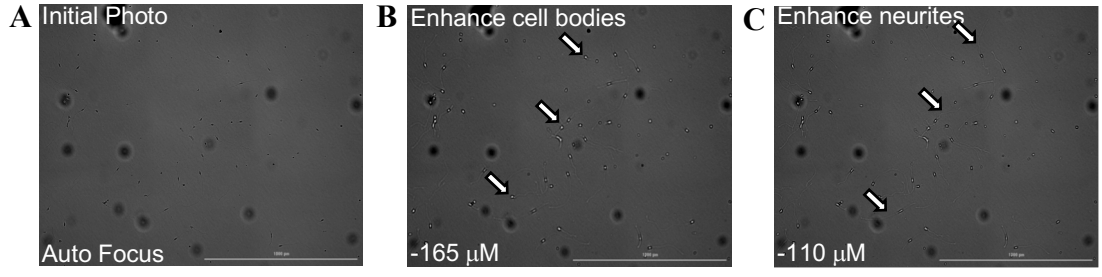

Figure 12: Images depicting necessary manual focus settings for automated imaging. (A): Shows the original autofocused image. (B): Shows the photo set to focus level -165µm relative to the auto-focused image for enhanced imaging of the cell bodies. (C): Shows the photo set focused to -110µm for enhanced imaging of the neurite outgrowths.

would be the most efficient. To accomplish this goal, CellProfiler, a cell image analysis software, was used to create a pipeline, or series of steps, to edit and measure the images to distinguish between the cell bodies and the neurite outgrowths. Using a standard auto focus image within this pipeline is insufficient due to the cell body and neurites being too out-of-focus for the program to accurately define the features of the cells. To enhance and bolden the border of the cell body, changing the focus to -165μm relative to the autofocus level was the preferred choice as shown in Figure 12B. Figure 12C different focus level set at -110μm was necessary to selectively enhance the neurites.

Figure 13A-C displays the current CellProfiler Pipeline. Figure 13A starts by bringing in three photos with the set focus levels that are shown in Figure 12. The fusion method is set to linear blending, which will combine the lines together when the images merge together in the end. Cropping was necessary to eliminate the border that is produced on the images when exported from Gen5. The photos are then labeled so separate parameters can be set. Figure 13B presents the settings necessary to optimize the definitions of the cell body. The cell bodies are shown brighter within the image compared to the background, so a dark background setting that is edited with the flattening and image smoothing steps, only the cell bodies defined will be selected during the object selection process. Flattening and smoothing enhances the background to eliminate noise. Since the cell bodies are a larger single area, a larger flattening size is used to selectively target them. Fine results set as a priority will yield the sharpest line during object selection. The steps shown in Figure 13C are optimized for selecting the neurite outgrowths. With this step it is unnecessary to entirely distinguish the separation of the cell body and the neurite outgrowths, since the cell body selection steps will be used for deselection in the end. The background flattening size is set to 5μm, since the neurites are significantly thinner than the cell bodies. Image smoothing was also applied to smooth the borders between the neurites and the cell bodies, as well as some of the neurites that split, since some portions were being counted as distinct objects. Figure 13D displays the analysis and processing steps, which start by selecting the defined objects in the neurite selection, then from that portion deselecting the defined areas in the cell body selection. Only the measurement of neurites will be selected in the end, which then will get a direct value calculated, representing a total measurement for all neurites in the well.

Figure 13:

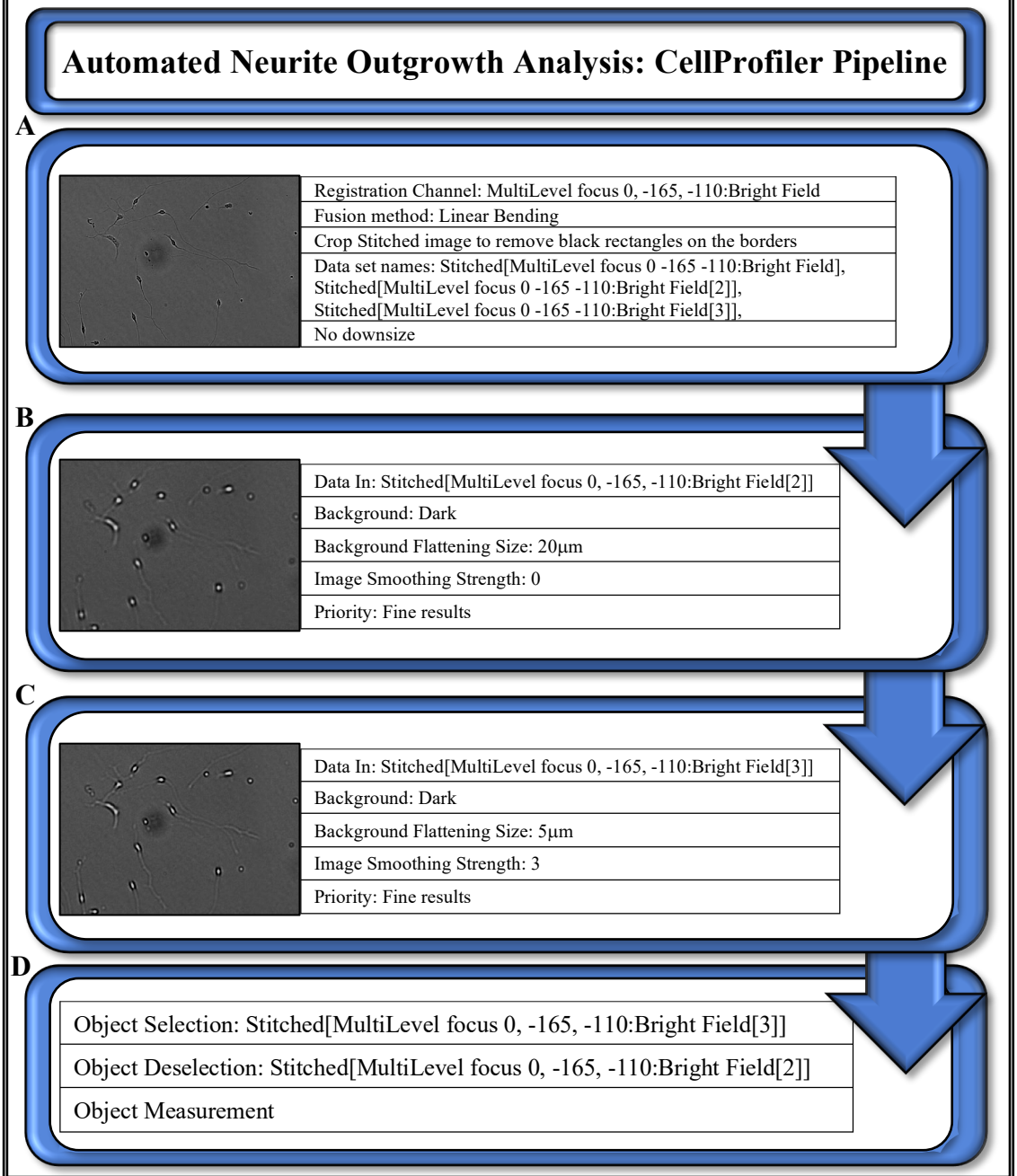

Figure 13: This figure defines the current pipeline steps that the software program CellProfiler executes in order to properly compute the final measurement analysis. (A): The program begins with an autofocus bright field image, setting the fusion method to linear blending, and cropping. Defining the names of the layers allowed for the program to separately apply different settings. (B): The program brings in the -165µm photo; parameters are defined as referenced for maximum cell body definition. (C): The -110µm photo has its parameters defined for optimal neurite specification. The measurements are then calculated after the defined features are automatically outlined. (D): Selects the neurite outgrowth borders, deselects the defined areas of the cell bodies, then outputs a calculated measurement.

Discussion

As for the cryopreservation analysis, two additional cell lines have been successfully thawed and plated after many cryopreservation trials. Unfortunately, due to contamination and robotic maintenance issues, full growth results from those attempts are unable to be created. Even though it has been successful with initial plating, integrating this automated cryopreservation script with the other two cell types has been shown to be less efficient compared to the 9-1 cell line. This is likely to be due to the use of ReLeSR as a passaging reagent, since results shown a lower initial density when compared to using the sodium citrate solution as a passaging reagent. Due to the small amount of liquid volume in the wells during the cell collection step, only a small amount of the cell solution can actually be transported from the well to the 15mL tube. Further, the ReLeSR passaging script requires a manual application of shear stress; this necessity for manual intervention is less than ideal, since the goal is to fully automate the process. Because of this inefficiency, incorporating the sodium citrate passaging sequence to replace the ReLeSR passaging protocol would be the next step in creating a more efficient cryopreservation script. Not only would the script be fully automated with no human interaction needed, the efficiency in transporting an increased number of cells into the cryopreservation solution would significantly improve the workflow.

Recreating the cellular growth curves, as well as subsequent immunostaining is also necessary to confirm that the iPSCs have retained their pluripotency characteristics. Along with that, testing the differentiation capabilities and subsequently staining those resulting cells would be another method of confirming the cells' retained pluripotency. Without these results it cannot be determined that the cells are keeping the phenotypes that were present before the cryopreservation was initiated.

Differentiation of the iPSCs into neurons and then cryopreservation of the developed neurons is critical in joining the two halves to this research. Plating the iPSCs onto a Laminin-coated plate as well as starting the differentiation process earlier is the next step in improving the protocol in producing more neurons that could be used for the drug screen. With the creation of the neurons finished, the cryopreservation of these cell types would need to be optimized, either using a manual protocol or an automated version. Attempting the automated cryopreservation script on the created neurons is another step

that needs to be performed to see if there would be success on this differentiated cell type, otherwise other cryopreservation methods, such as the standard DMSO cryopreservation, would have to be used.

Preferably, it would be most efficient to add an automated counting step into this process, either before cryopreservation to calculate a specific concentration of neurons per vial or during the thawing and plating process. The idea to implement an automated counting step turned out harder than initially believed since many factors are at play. An additional plate would be needed to be stored within the worktable area so that an aliquot could be distributed into in. Then the plate would have to be moved into the Cytation One cell imager with a custom counting protocol. Once the counting protocol has been executed, the cell number should be exported in an excel file. Ideally, the value that is exported could be imported into the script as a variable, however trying to incorporate a variable reliant on another program's export is difficult, since the file type of the export is not compatible with the type needed for referencing a variable. Additional cooperation with the Tecan team, and possibly the BioTek team if needed, would most likely solve this problem. Time and work priorities delayed this potential solution, since it wasn't of critical importance since there was a successful manual counting method in place.

The neurons that were partially characterized with immunocytochemistry were created using the same differentiation protocol that was used in this research. It is necessary to understand the phenotype of the manually-differentiated cells, so that proper comparison of the automated differentiated cells can occur. The presence of glutamate decarboxylase (GAD67) indicates the presence of the enzyme which converts glutamate to GABA. Between that and the presence of GABA Transporter 1 (GAT1) indicated that the neurons that were differentiated with this protocol are, at least partially, a GABAergic subtype of neurons. The presence of Glutamine Synthetase is slightly puzzling, since this enzyme is usually present in astrocytes when looking at cell types in the brain. With the few successful antibodies used within this research, it is not possible to exactly define the neuron subtype, and repetitions of this work will need to be performed.

Future work will also incorporate the automated drug screen that will be performed on these neurons. The neuronal plating and maintenance scripts will allow for the screen to run smoothly. The end goal would be to have an entirely automated pipeline from iPSC

thawing and plating, passaging and expanding, differentiation, cryopreservation, and finally running a drug screen experiment. With additional research to confirm the efficiency of cryopreservation, improve the neuronal freezing, and execute an experimental drug screen, a fully automatable and customizable drug screening platform would be able to be utilized to its full potential. The results of this research demonstrate the reduction in the amount of monotonous manual cell culture work technicians would be required to do when executing the pre-programmed protocol scripts. With more development and testing, a fully automated end-to-end cell culturing and screening workstation would be available to expand research opportunities without the use of a technician, allowing for researchers to spend less time focusing on the time-consuming task of maintaining cells.

References:

1. Takahashi, K., Tanabe, K., Ohnuki, M., Narita, M., Ichisaka, T., Tomoda, K., & Yamanaka, S. (2007). Induction of Pluripotent Stem Cells from Adult Human Fibroblasts by Defined Factors. *Cell*, *131*, 861-872. doi:10.1016/j.cell.2007.11.019

2. Kempner, M. E., & Felder, R. A. (2002). A Review of Cell Culture Automation. *JALA: Journal of the Association for Laboratory Automation*, *7*, 56–62. https://doi.org/10.1016/S1535-5535-04-00183-2

3. Thomas, R. J., Chandra, A., Hourd, P. C., & Williams, D. J. (2008). Cell Culture Automation and Quality Engineering: A Necessary Partnership to Develop Optimized Manufacturing Processes for Cell-Based Therapies. *JALA: Journal of the Association for Laboratory Automation, 13, 152-158.* https://doi.org/10.1016/j.jala.2007.12.003

4. Hussain, W., Moens, N., Veraitch, F. S., Hernandez, D., Mason, C., & Lye, G. J. (2013). Reproducible culture and differentiation of mouse embryonic stem cells using an automated microwell platform. *Biochemical Engineering Journal*, *77*, 246–257. https://doi.org/10.1016/j.bej.2013.05.008

5. Terstegge, S., Laufenberg, I., Pochert, J., Schenk, S., Itskovitz-Eldor, J., Endl, E., & Brüstle, O. (2007). Automated maintenance of embryonic stem cell cultures. *Biotechnology and Bioengineering*, *96*, 195-201. https://doi.org/10.1002/bit.21061

6. Parr, A. M., Walsh, P. J., Truong, V., & Dutton, J. R. (2015). cGMP-Compliant expansion of human iPSC cultures as adherent monolayers. Methods in Molecular Biology, 1357, 221-229. doi:10.1007/7651_2015_243

7. Badée, J., Qiu, N., Parrott, N., Collier, A. C., Schmidt, S., & Fowler, S. (2019). Optimization of experimental conditions of automated glucuronidation assays in human liver microsomes using a cocktail approach and ultra-high performance liquid chromatography–tandem mass spectrometry. *Drug Metabolism and Disposition*, *47*, 124–134. https://doi.org/10.1124/dmd.118.084301

8. Yu, Y., Li, Z., Guo, R., Qian, J., Zhang, H., Zhang, J., … Wang, Y. (2019). Ononin, sec-O-β-D-glucosylhamaudol and astragaloside I: antiviral lead compounds identified via high throughput screening and biological validation from traditional Chinese medicine Zhongjing formulary. *Pharmacological Research*, *145,* 1-11. https://doi.org/10.1016/j.phrs.2019.04.032

9. Hunt, C. J. (2011). Cryopreservation of human stem cells for clinical application: A review. *Transfusion Medicine and Hemotherapy*, 38, 107–123. https://doi.org/10.1159/000326623

10. Pegg, D. E. (2007). Principles of Cryopreservation. *Cryopreservation and Freeze-Drying Protocols*, 368, 39-57. doi:10.1007/978-1-59745-362-2_3

11. Meryman, H. T. (2007). Cryopreservation of living cells: principles and practice. *Transfusion*, *47*, 935–945. https://doi.org/10.1111/j.1537-2995.2007.01212.x

12. Lovelock, J. E. (1954). The protective action of neutral solutes against haemolysis by freezing and thawing. *The Biochemical Journal*, *56*, 265–270. https://doi.org/10.1042/bj0560265

13. Meryman, H. T. (1971). Osmotic stress as a mechanism of freezing injury. *Cryobiology*, *8*, 489–500. https://doi.org/10.1016/0011-2240(71)90040-X

14. Yuan, C., Gao, J., Guo, J., Bai, L., Marshall, C., Cai, Z., … Xiao, M. (2014). Dimethyl sulfoxide damages mitochondrial integrity and membrane potential in cultured astrocytes. *PLOS ONE*, *9,* 1-9. https://doi.org/10.1371/journal.pone.0107447

15. Lovelock, J. E., & Bishop, M. W. H. (1959). Prevention of Freezing Damage to Living Cells by Dimethyl Sulphoxide. *Nature*, *183*, 1394–1395. https://doi.org/10.1038/1831394a0

16. Notman, R., Den Otter, W. K., Noro, M. G., Briels, W. J., & Anwar, J. (2007). The permeability enhancing mechanism of DMSO in ceramide bilayers simulated by molecular dynamics. *Biophysical Journal*, *93*, 2056–2068. https://doi.org/10.1529/biophysj.107.104703

17. Galvao, J., Davis, B., Tilley, M., Normando, E., Duchen, M. R., & Cordeiro, M. F. (2014). Unexpected low-dose toxicity of the universal solvent DMSO. *The FASEB Journal*, *28*, 1317–1330. https://doi.org/10.1096/fj.13-235440

18. Hanslick, J. L., Lau, K., Noguchi, K. K., Olney, J. W., Zorumski, C. F., Mennerick, S., & Farber, N. B. (2009). Dimethyl sulfoxide (DMSO) produces widespread apoptosis in the developing central nervous system. *Neurobiology of Disease*, *34*, 1–10. https://doi.org/10.1016/J.NBD.2008.11.006

19. Katkov, I. I., Kim, M. S., Bajpai, R., Altman, Y. S., Mercola, M., Loring, J. F., … Levine, F. (2006). Cryopreservation by slow cooling with DMSO diminished production of Oct-4 pluripotency marker in human embryonic stem cells. *Cryobiology*, *53*, 194–205. https://doi.org/10.1016/j.cryobiol.2006.05.005

20. Verheijen, M., Lienhard, M., Schrooders, Y., Clayton, O., Nudischer, R., Boerno, S., … Caiment, F. (2019). DMSO induces drastic changes in human cellular processes and epigenetic landscape in vitro. *Scientific Reports*, *9,* 1-12. https://doi.org/10.1038/s41598-019-40660-0

21. Crowe, J. H., & Crowe, L. M. (2000). Preservation of mammalian cells - Learning nature's tricks. *Nature Biotechnology*, *18*, 145–146. https://doi.org/10.1038/72580

22. Dobrynin, A. V., Colby, R. H., & Rubinstein, M. (2004). Polyampholytes. *Journal of Polymer Science, Part B: Polymer Physics*, *42*, 3513–3538. https://doi.org/10.1002/polb.20207

23. Matsumura, K., Bae, J. Y., & Hyon, S. H. (2010). Polyampholytes as cryoprotective agents for mammalian cell cryopreservation. *Cell Transplantation*, *19*, 691–699. https://doi.org/10.3727/096368910X508780

24. Svalgaard, J. D., Talkhoncheh, M. S., Haastrup, E. K., Munthe-Fog, L., Clausen, C., Hansen, M. B., … Fischer-Nielsen, A. (2018). Pentaisomaltose, an Alternative to DMSO. Engraftment of Cryopreserved Human CD34+ Cells in Immunodeficient NSG Mice. *Cell Transplantation*, *27*, 1407–1412. https://doi.org/10.1177/0963689718786226

25. Pollock, K., Budenske, J. W., McKenna, D. H., Dosa, P. I., & Hubel, A. (2017). Algorithm-driven optimization of cryopreservation protocols for transfusion model cell types including Jurkat cells and mesenchymal stem cells. *Journal of Tissue Engineering and Regenerative Medicine*, *11*, 2806–2815. https://doi.org/10.1002/term.2175

26. Macfarlane, S. R., Seatter, M. J., Kanke, T., & Hunter, G. D. (2001). Proteinase-Activated Receptors*, Pharmacological Reviews, 53,* 245-282. Retrieved from http://pharmrev.aspetjournals.org

27. Han, K. S., Mannaioni, G., Hamill, C. E., Lee, J., Junge, C. E., Lee, C. J., & Traynelis, S. F. (2011). Activation of protease activated receptor 1 increases the excitability of the dentate granule neurons of hippocampus. *Molecular Brain*, *4,* 1-12. https://doi.org/10.1186/1756-6606-4-32

28. Ye L, S Zhang, L Greder, J Dutton, SA Keirstead, M Lepley, L Zhang, D Kaufman and J Zhang. (2013). Effective cardiac myocyte differentiation of human induced pluripotent stem cells requires VEGF. *PLOS One, 8*, 1-10. doi:10.1371/journal.pone.0053764

29. Noorbakhsh, F., Vergnolle, N., Hollenberg, M. D., & Power, C. (2003). Proteinase-activated receptors in the nervous system. *Nature Reviews Neuroscience*, 4, 981–990. https://doi.org/10.1038/nrn1255

30. Scarisbrick, I. A. (2008). The multiple sclerosis degradome: enzymatic cascades in development and progression of central nervous system inflammatory disease. *Current Topics in Microbiology and Immunology*, *318*, 133–175. https://doi.org/10.1007/978-3-540-73677-6_6

31. Whetstone, W. D., Walker, B., Trivedi, A., Lee, S., Noble-Haeusslein, L. J., & Hsu, J. C. (2017). Protease-Activated Receptor-1 Supports Locomotor Recovery by Biased Agonist Activated Protein C after Contusive Spinal Cord Injury. *PLOS ONE, 12*, 1-18. doi:10.1371/journal.pone.0170512

32. Molino, M., Barnathan, E. S., Numerof, R., Clark, J., Dreyer, M., Cumashi, A., … Brass, L. F. (1997). Interactions of mast cell tryptase with thrombin receptors and PAR-2. *Journal of Biological Chemistry*, *272*, 4043–4049. https://doi.org/10.1074/jbc.272.7.4043

33. Wilson, S., Greer, B., Hooper, J., Zijlstra, A., Walker, B., Quigley, J., & Hawthorne, S. (2005). The membrane-anchored serine protease, TMPRSS2, activates PAR-2 in prostate cancer cells. *Biochemical Journal*, *388*, 967–972. https://doi.org/10.1042/BJ20041066

34. Posma, J. J., Grover, S. P., Hisada, Y., Owens, A. P., Antoniak, S., Spronk, H. M., & Mackman, N. (2019, January 1). Roles of Coagulation Proteases and PARs (Protease-Activated Receptors) in Mouse Models of Inflammatory Diseases. *Arteriosclerosis, Thrombosis, and Vascular Biology*, *39*, 13–24. https://doi.org/10.1161/ATVBAHA.118.311655

35. Semeraro, F., Ammollo, C. T., Morrissey, J. H., Dale, G. L., Friese, P., Esmon, N. L., & Esmon, C. T. (2011). Extracellular histones promote thrombin generation through platelet-dependent mechanisms: Involvement of platelet TLR2 and TLR4. *Blood*, *118*, 1952–1961. https://doi.org/10.1182/blood-2011-03-343061

36. Chen, R., Kang, R., Fan, X. G., & Tang, D. (2014). Release and activity of histone in diseases. *Cell Death and Disease*, *5*, 1-9. https://doi.org/10.1038/cddis.2014.337

37. Thorsen, K., Ringdal, K. G., Strand, K., Søreide, E., Hagemo, J., & Søreide, K. (2011, July). Clinical and cellular effects of hypothermia, acidosis and coagulopathy in major injury. *British Journal of Surgery*, *98*, 894–907. https://doi.org/10.1002/bjs.7497

38. Suidan, H. S., Stone, S. R., Hemmings, B. A., & Monard, D. (1992). Thrombin causes neurite retraction in neuronal cells through activation of cell surface receptors. *Neuron*, *8*, 363–375. https://doi.org/10.1016/0896-6273(92)90302-T

39. Turgeon, V. L., Lloyd, E. D., Wang, S., Festoff, B. W., & Houenou, L. J. (1998). Thrombin Perturbs Neurite Outgrowth and Induces Apoptotic Cell Death in Enriched Chick Spinal Motoneuron Cultures through Caspase Activation. *The Journal of Neuroscience*, *18*, 6882–6891. https://doi.org/10.1523/JNEUROSCI.18-17-06882.1998

40. Hamill, C. E., Mannaioni, G., Lyuboslavsky, P., Sastre, A. A., & Traynelis, S. F. (2009). Protease-activated receptor 1-dependent neuronal damage involves NMDA receptor function. *Experimental Neurology*, *217*, 136–146. https://doi.org/10.1016/j.expneurol.2009.01.023

41. Lee, C. J., Mannaioni, G., Yuan, H., Woo, D. H., Gingrich, M. B., & Traynelis, S. F. (2007). Astrocytic control of synaptic NMDA receptors. *J Physiol*, *581*, 1057–1081. https://doi.org/10.1113/jphysiol.2007.130377

42. Kermer, P., Klöcker, N., & Bähr, M. (1999). Neuronal death after brain injury. Cell and Tissue Research, 298, 383-395. doi:10.1007/s004410050061

43. Choi, C., Yoon, H., Drucker, K. L., Langley, M. R., Kleppe, L., & Scarisbrick, I. A. (2018). The Thrombin Receptor Restricts Subventricular Zone Neural Stem Cell Expansion and Differentiation. *Scientific Reports, 8,* 1-15. doi:10.1038/s41598-018-27613-9

44. Radulovic, M., Yoon, H., Wu, J., Mustafa, K., & Scarisbrick, I. A. (2016). Targeting the thrombin receptor modulates inflammation and astrogliosis to improve recovery after spinal cord injury. Neurobiology of Disease, 93, 226-242. doi:10.1016/j.nbd.2016.04.010

45. Geng, Z., Walsh, P. J., Truong, V., Hill, C., Ebeling, M., Kapphahn, R. J., … Dutton, J. R. (2017). Generation of retinal pigmented epithelium from iPSCs derived from the conjunctiva of donors with and without age related macular degeneration. *PLOS ONE, 12,* 1-20. doi:10.1371/journal.pone.0173575